Available online at www.sciencedirect.com

SciVerse ScienceDirect

journal homepage: www.elsevier.com/locate/he

Review

Review of hydrogen storage techniques for on board vehicle applications

*D.J. Durbin, C. Malardier-Jugroot**

Department of Chemistry and Chemical Engineering, Royal Military College of Canada, Kingston K7L7B4, Canada

ARTICLE INFO

Article history:
Received 11 March 2013
Accepted 17 July 2013
Available online 4 October 2013

Keywords:
Hydrogen storage
Chemical hydrides
Adsorption materials
Metal-organic frameworks
Carbon
Nanostructures

ABSTRACT

Hydrogen gas is increasingly studied as a potential replacement for fossil fuels because fossil fuel supplies are depleting rapidly and the devastating environmental impacts of their use can no longer be ignored. H_2 is a promising replacement energy storage molecule because it has the highest energy density of all common fuels by weight. One area in which replacing fossil fuels will have a large impact is in automobiles, which currently operate almost exclusively on gasoline. Due to the size and weight constraints in vehicles, on board hydrogen must be stored in a small, lightweight system. This is particularly challenging for hydrogen because it has the lowest energy density of common fuels by volume. Therefore, a lot of research is invested in finding a compact, safe, reliable, inexpensive and energy efficient method of H_2 storage. Mechanical compression as well as storage in chemical hydrides and absorption to carbon substrates has been investigated. An overview of all systems including the current research and potential benefits and issue are provided in the present paper.

1. Introduction

Human society currently relies primarily on fossil fuels for energy production. This energy storage medium is so effective that it spurred the Industrial Revolution. However, in the 21st century, it is clear that fossil fuels cannot continue to be the primary energy source because resources are rapidly depleting and significant emissions of greenhouse gases result from fossil fuel burning. As a result, a cleaner, more sustainable energy source is being actively pursued [1,2].

One of the largest users of fossil fuels is motorized vehicles, which burn gasoline in an internal combustion engine (ICE). The first attempt to limit the use of fossil fuels in automobiles was the development of hybrid vehicles, which contain a battery that carries an electric charge in addition to an ICE. Hybrid vehicles have had some success but they are not a solution because they still require some input of fossil fuels. As a result, the next generation of automobiles will likely be fuel cells vehicles (FCV). FCVs take in hydrogen gas to power a hydrogen fuel cell, such as a polymer electrolyte membrane fuel cell. These vehicles are desirable because they produce no environmentally damaging emissions. In addition, once a sustainable method for H_2 gas production is developed, FCVs will have a constant fuel supply [3].

At 143.0 MJ/kg, hydrogen has the highest energy density of common fuels by weight (three times larger than gasoline) [4]. Unfortunately, at 0.0108 MJ/L, gaseous H_2 also has the lowest energy density by volume (over 3000 times smaller than

* *Corresponding author*. Tel.: +1 6135416000.
E-mail address: Cecile.Malardier-Jugroot@rmc.ca (C. Malardier-Jugroot).
0360-3199/$ – see front matter
http://dx.doi.org/10.1016/j.ijhydene.2013.07.058

gasoline) (Fig. 1) and it can explode violently when brought into contact with air. There is limited space to store fuel on a vehicle and the fuel tank must be reinforced enough to prevent explosion during a crash. Therefore, a compact, safe, reliable, inexpensive and energy efficient method of storing H_2 is needed if FCVs are to become commonly used. In addition, the tank must hold enough hydrogen for the automobile to travel ca. 500 km between fills [5].

Hydrogen gas storage is very difficult because, being the smallest molecule, H_2 is highly diffuse and buoyant. Although it has been stored in the gaseous form for centuries and as a liquid since the 1940's, traditional mechanical means of H_2 storage (compression and liquefaction) are very energetically and financially expensive. As a result, many alternative storage methods are being extensively researched. These include cryocompression as well as storage within chemical hydrides and absorption to bulk carbon substrates. The hydrogen storage capacity of commonly-used materials is shown in Fig. 2 [3].

In 2003, the US Department of Energy (DOE), released targets for hydrogen storage systems at five year intervals beginning in 2005 and continuing to ultimate goals. The DOE targets consider volumetric and gravimetric capacities, refuelling time, costs, cycle life and loss of usable hydrogen. Wherever possible, this paper has included analysis of each storage mechanism according to DOE targets. In specific, the volumetric and gravimetric capacities are considered along with cost and efficiency. DOE analyses are most readily available for mechanical methods of hydrogen storage because they are the most traditional storage methods and so were the first to be investigated.

Gravimetric capacity is the amount of electricity produced by a given weight of fuel; volumetric capacity is the amount of gas present in a given volume. High values of both are desired [7]. Both measurements must include the fuel and storage container. Rankings of many hydrogen storage methods according to gravimetric and volumetric capacities are shown in Fig. 3, along with the 2015 and ultimate DOE targets.

As can be seen from Fig. 3, no hydrogen storage technology currently meets DOE standards. This is because each storage mechanism has fundamental limits: gaseous H_2 requires a large volume; liquid hydrogen evaporates easily; metal hydrides add significant weight to the system and adsorbent materials do not hold enough hydrogen. Therefore, research is constantly underway to improve these storage techniques and develop new storage mechanisms [9]. The current options for storage on board FCVs are discussed in the following three sections.

2. Mechanical storage

Mechanical hydrogen storage methods contain hydrogen in an unbound and unaltered form. Such methods of compression and cryogenic cooling (Sections 2.1 and 2.2) were used historically to increase the volumetric and gravimetric capacity of H_2. Recently, this has progressed to combined cryocompression

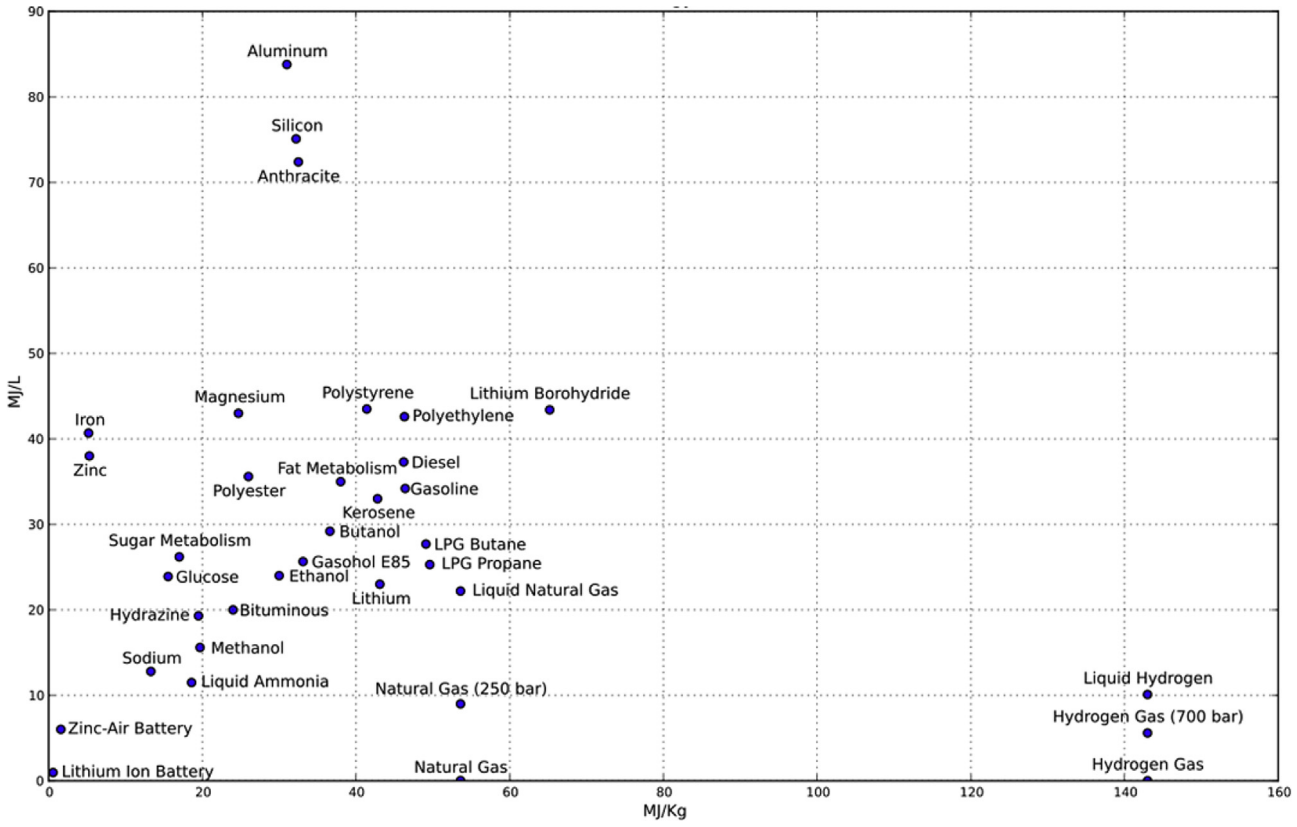

Fig. 1 – Comparison of energy densities by weight (MJ/kg) versus volume (MJ/L) for many common fuels and other useful materials (New Energy and Fuel, 2009 from data by Eberhardt 2002 [6]).

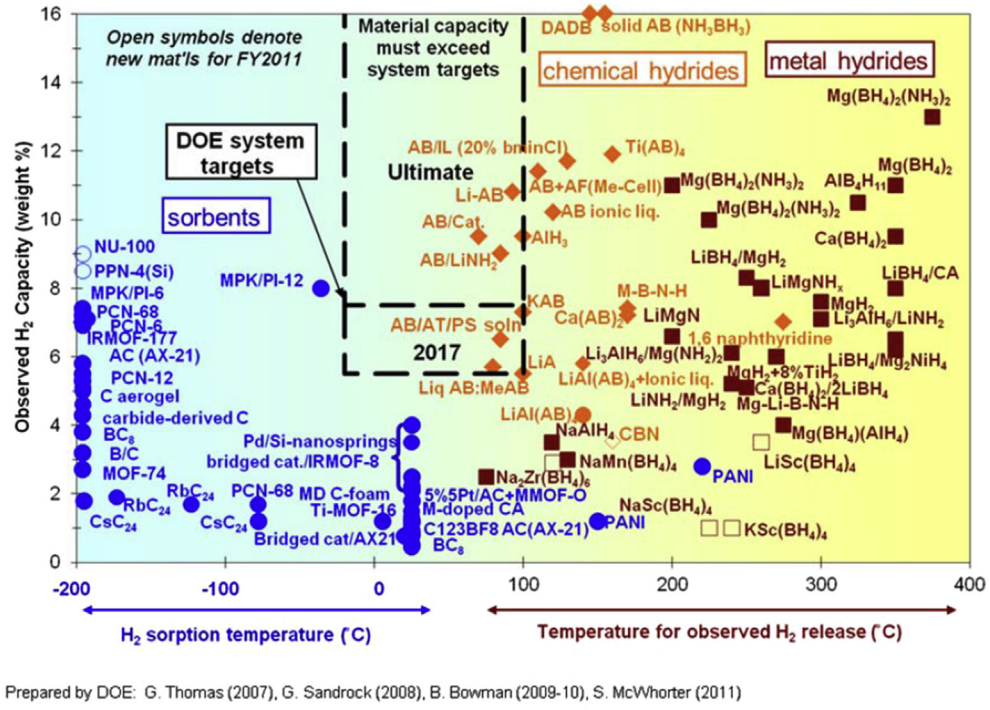

Fig. 2 – Hydrogen storage capacity of commonly used materials with respect to operating temperature. Reprinted with permission from S. Satyapal, U.S. Department of Energy.

mechanisms (Section 2.3). Mechanical methods are currently the most common means of hydrogen storage.

2.1. *Compressed gas*

2.1.1. *High-pressure tanks*

The most commonly used method of hydrogen storage in fuel cell vehicles is compressed hydrogen tanks. This method has been chosen because at present it is the best understood. Many variables must be considered before high-pressure storage becomes a viable option. These include weight, volume, cost and safety [3].

The most important consideration for compressed H_2 storage is the material composing the high-pressure vessel. It must be able to withstand the embrittlement possible with hydrogen in addition to being lightweight, inexpensive and easy to work with. Vessels were originally made from aluminium, which is ideal for construction and has a high

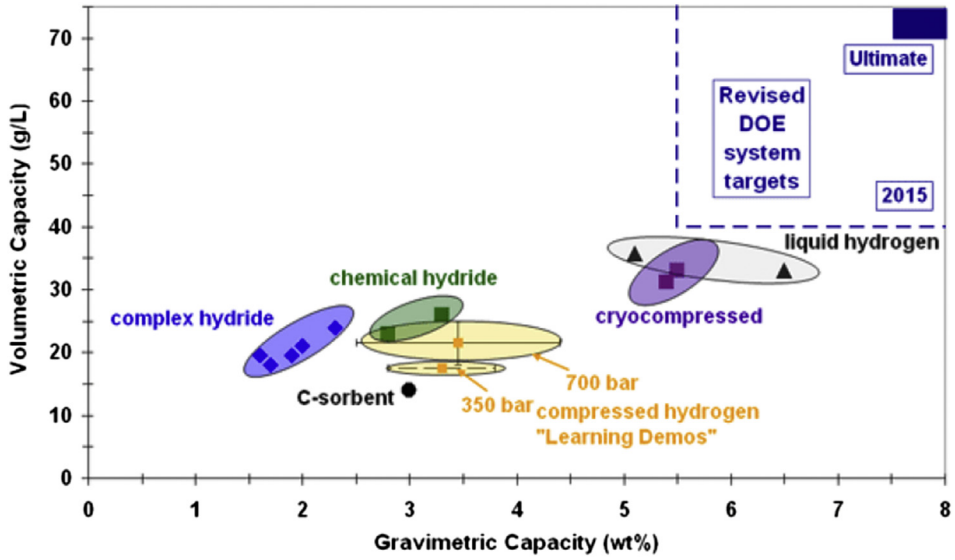

Fig. 3 – Ranking of current hydrogen storage technologies by volumetric and gravimetric capacities showing the DOE 2015 and ultimate targets. Reprinted from Ref. [8] Satyapal 2007 with permission.

thermal conductivity. However, aluminium vessels were not strong enough and often could not comply with safety standards. Therefore, the vessel material has changed to a carbon fibre/epoxy composite (carbon fibre reinforced plastic, CFRP) in recent years [3,10].

CFRP vessels are lightweight and very strong, but they have relatively low thermal conductivity. Therefore, the material must be kept below 358 K at all times to comply with safety requirements. This temperature constraint can be an issue, especially during filling the tank when the exothermic compression of the gas causes the temperature to rise drastically. The CFRP unit is also sensitive to fire and high temperatures, which cause a degradation of its mechanical properties. There is a large concern that an explosion would result if the H_2 storage vessel was subjected to a fire, such as might occur in a car crash [5,11].

At present, two types of tanks are commonly used: type IV is composed entirely of CFRP; type III contains metal-lined CPRP and so encompasses properties of both the early aluminium tanks and the currently used CFRP tanks. Type III is preferred, but its cost is prohibiting. As a result, alternative tanks under investigation. One such system is discussed below [3].

An alternative to the currently used type III and IV vessels is a CFRP tank reinforced with a space-filling skeleton. This tank will use struts and web elements in tension to resist the force of compressed gas. Addition of the skeleton should allow for lighter, stronger tanks designed in any shape (current tanks must be round in order to achieve a high membrane resistance and low surface-to-volume ratio). However, they will not become a viable technology until the manufacturing process and long-term system durability are improved [3,12].

Returning to current H_2 storage tanks, in 2009 the DOE Hydrogen Program analyzed the potential for on board H_2 storage in type IV tanks containing 5.6 kg of recoverable H_2. The current values and target of the four main criteria are discussed below.

Gravimetric capacity: A 345 atm tank was found to have a gravimetric capacity of 5.5 wt% (6.9 wt% in physically perfect conditions). A 690 atm tank was less weight efficient with a gravimetric capacity of 5.2 wt% (theoretical potential of 6.5 wt %). It is unlikely to meet the ultimate DOE target of 7.5 wt% for either tank [7].

Volumetric capacity: A 345 atm tank was found to have a volumetric capacity of 17.6 g H_2/L (18.6 g/L if the empty tank pressure is reduced to 3 atm). This will not even reach the 2010 DOE target of 28 g/L. A 690 atm tank was more volume efficient with a volumetric capacity of 26.3 g/L (possible increase to 27.2 g/L). This system will not reach the ultimate DOE target of 70 g/L [7].

Cost: The manufacturing costs were \$15.4/kWh for the 345 atm tank and \$18.7/kWh for the 690 atm tank. These are over four times the target of \$4/kWh. The cost of compressed H_2 fuel was \$4.22/gge for the 345 atm tank and \$4.33/gge for the 690 atm tank where gge is a gasoline gallon equivalent. This is approximately two times larger than the \$2.30/gge target [7].

Efficiency: The 345 atm compressed gas tank had an efficiency of 56.5%; the 690 atm tank had the slightly lower efficiency of 54.2%. Both values are within reach of the 60% DOE target [7].

Of the four obstacles discussed, cost is considered the greatest barrier. It is largely contributed to the carbon fibre composing the tank with a large contribution from assembly and some for binding. Even if the cost is lowered, there is concern that high-pressure tanks will not be accepted by the general public because they are perceived as unsafe [3].

2.1.2. *Capillary storage*

An alternative option for compressed hydrogen storage is capillaries or microspheres. These vessels are advantageous because (i) they require less hydrogen infrastructure because the capillaries will be filled at the fuel plant before delivery to the filling station; (ii) capillaries are safer because each one acts as an individual high-pressure vessel containing only a small amount of H_2; (iii) the system is lightweight because minimal material is required for each capillary and many can be stored together in a larger thin tank [15, 3].

At present, capillary H_2 storage greatly exceeds DOE targets in many areas. In addition to high gravimetric capacity, capillaries should be able to store enough H_2 to travel over 500 km in a 60 L tank that weighs only 50 kg by 2015. However, capillary storage does not meet the DOE targets for volumetric capacity and a large amount of energy is needed to release H_2 from the capillaries. The systems also have limited long term durability. Therefore, they are not currently in use [3,15].

2.2. *Cryogenic storage: liquid hydrogen*

Liquefying hydrogen is a means of increasing volumetric energy density. It is also called cryogenic storage because liquefaction is performed by cooling H_2 to 20 K. Although it is an energy expensive process, it increases H_2 volumetric energy density from 2.5 or 5 MJ/L (for compressed H_2 at 345 and 690 atm respectively) to 8 MJ/L (for liquid hydrogen LH_2). As a result, less volume is required for storage so a smaller, lighter container can be used. This allows longer distances to be driven (Fig. 4). Because of this great potential, LH_2 storage was extensively studied in the 1980's and 1990's [13].

If hydrogen is stored in the liquid form on board a FCV, it must be maintained below its boiling point of 20 K. Therefore, heat intrusion must be kept at the lowest possible level. To accomplish this, the original LH_2 tanks were metallic double-walled vessels. The inner vessel had multilayer insulation composed of several metallic foil layers separated by glass wool; space between the inner and outer vessels was evacuated to create a vacuum. This storage system is often referred to as vacuum superinsulation (Fig. 5). In recent years, pressure release valves have been added for safety reasons. In addition, new tanks must be able to release gaseous H_2 as well as LH_2. A LH_2 tank was most recently tested in a GM HydroGen3; it was found to hold 4.6 kg of LH_2 with a total system weight of 90 kg [13,14].

Despite important improvements to volumetric density, LH_2 storage is not frequently used for several reasons. First, at least 35% of the fuel's energy content is used to liquefy it. This is three times more energy than is needed to compress H_2 to 690 atm. Second, LH_2 evaporates very easily during delivery and refuelling. Third, LH_2 pressurizes quickly while on-board vehicles as it absorbs heat from the environment. Therefore, the tank must be vented every 3–5 days during inactivity to prevent dangerous and costly boil-off losses; if boil-off is not

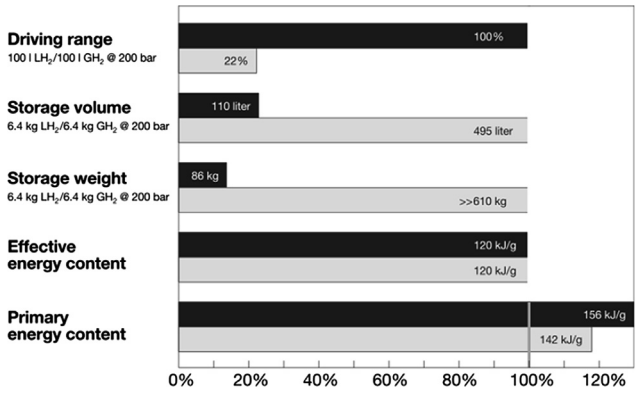

Fig. 4 – Comparison of compressed gaseous H_2 (GH_2; grey) and liquid H_2 (LH_2; black) based on driving range, storage volume, storage weight, effective energy content and primary energy content where the primary energy content is the energy required to compress or liquefy H_2. Reprinted from Ref. [13] with permission.

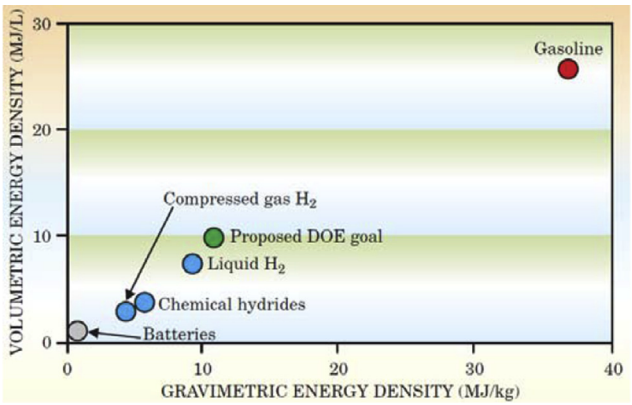

Fig. 6 – Volumetric energy density (MJ/L) versus gravimetric energy density (MG/kg) for several common fuels. Reprinted from Ref. [16] with permission.

controlled, the entire hydrogen store will evaporate in ca. 2 weeks. Even if these problems could be overcome, the volumetric energy density of LH_2 (ca. 8 MJ/L) is substantially less than that of gasoline (32 MJ/L) and diesel fuel (36 MJ/L) (Fig. 6). As a result, studies of mechanical hydrogen storage have largely shifted to cryocompressed H_2 (Section 2.3) in recent years [9,14–16].

2.3. *Cryocompressed hydrogen*

The newest hydrogen storage technologies combine compression and cryogenic storage of H_2 to produce cryocompressed hydrogen. This includes pressurized liquid hydrogen, cooled compressed hydrogen gas and two phase systems of liquid hydrogen with vapour in the headspace [17].

2.3.1. *Compressed liquid hydrogen*

The storage density of LH_2 is higher in insulated pressure vessels because it is slightly compressible: at 21 K, its density increases from 70 g/L at 1 atm to 87 g/L at 237 atm [17].

Cryocompressed vessels are preferred over traditional LH_2 storage containers because they are better able to withstand heat since H_2 within the vessel can be vented at a higher temperature. Venting stops when the tank reaches ambient temperature. When this occurs, the pressure within the tank is maintained so that the H_2 density remains at 30% of the initial LH_2 density. This is better for storage and makes the tanks much safer during dormant periods. In addition, cryocompressed H_2 vessels have the potential to increase the volumetric energy density by eliminating unused space in the container. This can be done because H_2 becomes a supercritical fluid at pressures greater than 13 atm before the tank must be vented [17].

A sophisticated cryogenic capable pressure vessel (Fig. 7) was recently developed at the Lawrence Livermore National Laboratory (LLNL) in California, USA. It has a high storage capacity (5–10× greater than conventional LH_2 tanks), long thermal endurance and flexible refuelling. In addition, this vessel eliminates the evaporative losses common in traditional liquid hydrogen tanks [9].

A model cryogenic pressure vessel placed in a Toyota Prius and fuelled with LH_2 showed the longest unrefueled driving

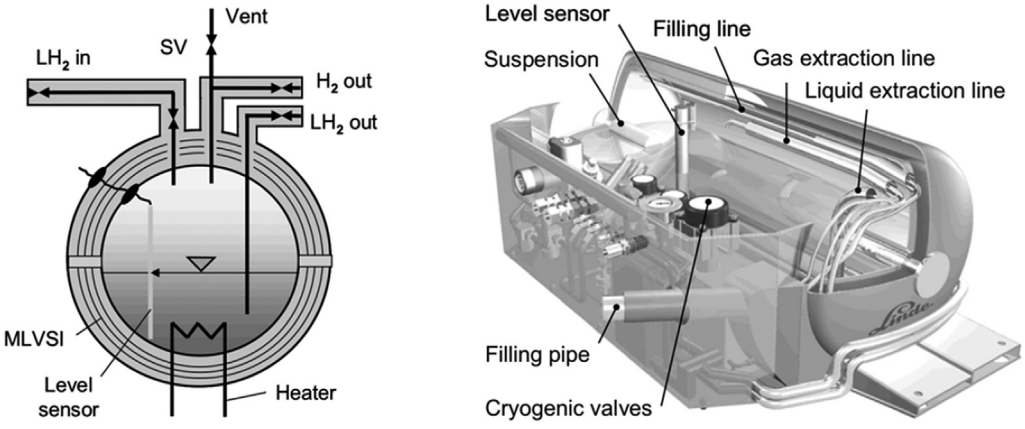

Fig. 5 – Liquid hydrogen storage tank showing the LH_2 storage vessel (left) and the full system (right). Reprinted from Ref. [14] with permission.

distance and most lengthy hold time without evaporative losses compared to other mechanical H_2 storage vessels. When cryocompressed H_2 storage was compared to DOE targets, it performed better than traditional compressed H_2 (Section 2.1) [9,17]. A tank containing 5.6 kg of recoverable H_2 at 71 g/L was assessed based on the following four criteria.

Gravimetric capacity: The tank had a gravimetric capacity of 5.5 wt% with a potential capacity of 6.5 wt% at higher pressures and 9.2 wt% if the shell was made from an aluminium alloy instead of steel and the liner thickness was reduced. Therefore, it can meet the DOE ultimate target of 7.5 wt% [17].

Volumetric capacity: The tank had a volumetric capacity of 41.8 g H_2/L with a potential of 47.8 g H_2/L at higher pressures. This easily complies with the DOE 2015 target of 40 g H_2/L, but cannot meet the ultimate target of 70 g H_2/L [17].

Cost: The manufacturing cost was \$12/kWh, which decreased to \$8/kWh for a larger prototype system containing 10.4 kg of useable hydrogen. This is still 2× larger than the DOE 2015 target of \$4/kWh. Furthermore, the fuel cost was \$4.57/gge, which is also 2× larger than the DOE target of \$2.30/gge [17].

Efficiency: The well-to-tank efficiency was 41.4%. This cannot meet the DOE target of 60% [17].

Despite the current shortcomings, compressed LH_2 storage vessels are amongst the most promising physical storage systems for hydrogen and so continue to undergo extensive study.

2.3.2. *Compressed cryogenic gas*

Cooling compressed hydrogen gas is advantageous because the gas becomes denser at colder temperatures, which allows more hydrogen to be stored in a tank without changing its size. Because the system does not need to be cooled to the temperature of liquid H_2 (20 K), this requires less energy than LH_2 storage.

Compressed hydrogen gas tanks are often cooled to 77 K with liquid nitrogen. This increases the volumetric capacity by three times compared to non-cooled hydrogen. It has been found that 740 atm is required to store 4.1 kg of hydrogen in 100 L at room temperature but only 148 atm is required to store the same volume at 77 K. While this is generally worthwhile, it should be noted that cooling a compressed gas increases the size and weight of the containment vessel because it must include thermal insulation [8,18].

Continued research into compressed cryogenic hydrogen storage led to the incorporation of adsorbents, which further decreased the storage pressure. For example, in the 100 L vessel discussed above, only 59 atm is required to store 4.1 kg H_2 if the vessel is filled with superactivated carbon pellets [18].

In a separate system, hydrogen adsorption at 77 K was analyzed on several carbon substrates. It was found that a maximum H_2 adsorption capacity of 5.2% (1.3 wt% below the ultimate DOE target) was obtained at 29 atm on substrates with high micropore density. This pressure is much lower than the previously-thought realistic range of 80–207 atm. Therefore, it is hoped that more research into hydrogen adsorption at 77 K will enable these systems to be brought to DOE standards [19]. Hydrogen storage by absorbents is further discussed in Section 4.

3. Chemical hydrides

The first type of non-mechanical hydrogen storage discussed in this paper is that within hydrides. Chemical hydrides are materials that contain chemically bound hydrogen. They are not rechargeable on board a fuel cell vehicle, so hydrides are not an ideal storage medium. However, they can store large amounts of hydrogen and so are worth considering. In addition, hydride storage can be very useful for large systems that would not refuel on board even if the option was available, such as rockets and jets, and single-use applications, such as batteries. Chemical hydrides are often favoured over adsorption storage (Section 4) because chemisorbed hydrogen has a

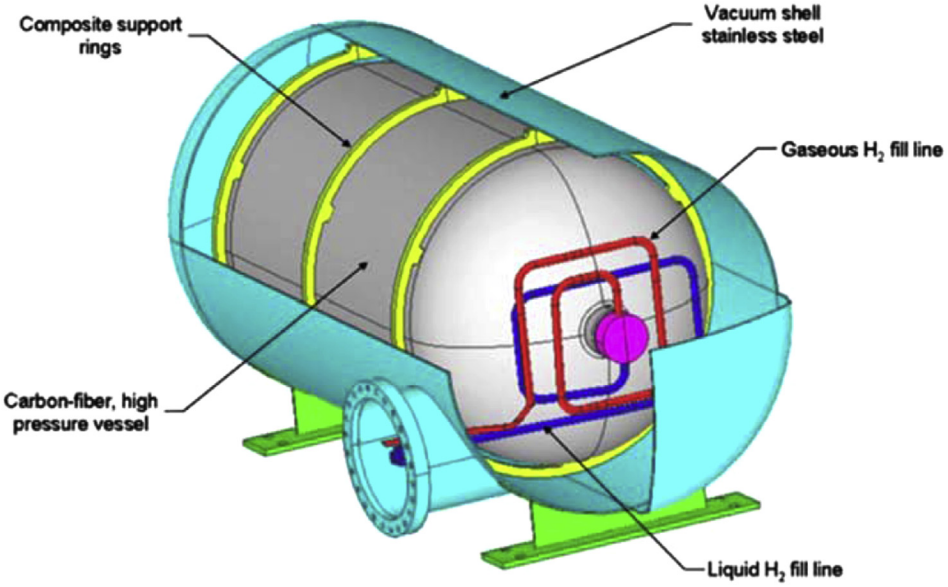

Fig. 7 – Cryogenic capable pressure vessel. Reprinted from Ref. [9] with permission.

binding energy of 2–3 eV, while that in physisorbed hydrogen is only 0.1 eV [3,20,21].

There are two main classes of hydrides: those that contain metals and those that are composed entirely of non-metals. These discussed in Sections 3.1 and 3.2 respectively.

3.1. *Metal hydrides*

Metal hydrides have been given a lot of attention recently because they often have higher volumetric and gravimetric content than mechanical storage methods (Table 1). In addition, hydrides can operate at the relatively low temperatures and pressures required in fuel cell vehicles, (the optimum ranges being 1–10 atm and 25–393 K for a PEMFC) [8].

3.1.1. *Simple metal hydrides*

Simple metal hydrides are metal complexes that incorporate hydrogen into their crystal structure. They have been investigated since 1866 when Thomas Graham observed hydrogen absorption onto palladium. Metal hydrides are divided into two classes: binary hydrides, which contain only one metal in addition to hydrogen with the formula MH_x (M = metal), and intermetallic hydrides, which contain two or more metals. Two-metal hydrides have the general formula $A_mB_nH_x$ where A and B are metals; they are then further subdivided into AB_5 ($CaCu_5$ structure type), AB_2 (Laves phase), AB (CsCl structure type) or A_2B (AlB_2 structure type) where metal A has a strong affinity for hydrogen and forms a stable binary hydride while metal B does not interact with hydrogen [22].

For a simple metal hydride to be practical for hydrogen storage, it must be produced by an exothermic reaction. The kinetics of the reaction must favour low energy hydride formation and H_2 desorption [21].

3.1.1.1. Binary metal hydrides. There are many binary metal hydrides. However, most are not discussed here because they have such low gravimetric capacity that their use is unrealistic. The most promising binary metal hydride is alane (aluminium hydride, AlH_3), which contains 10.1 wt% hydrogen with a density of 1.48 g/mL. There are at least seven phases of thermodynamically unstable alane that are metastable at room temperature and so do not decompose rapidly. Some level of instability is necessary for hydrogen storage materials because they must be able to release hydrogen without a large energy input [21].

The size of the metal hydride particles has a large effect on the thermodynamics and kinetics of hydrogen adsorption and desorption. It had previously been noted that reducing the particle size to the nanoscale lowers the desorption temperature and accelerates reaction kinetics. This occurs because (i) the surface-to-volume ratio increases, which increases surface reactions such as adsorption and desorption, and (ii) defects are formed, which cause the material to become more amorphous (less crystalline), which leads to more favourable thermodynamics [21].

Further research into the effect of size on hydrogen storage in alane lead to density functional theory (DFT) calculations performed on clusters containing 1–20 aluminium atoms. These studies found that, with the exception of very small clusters, desorption energy decreases steadily as cluster size increases until it reaches the low value of 0.19 eV/H_2 for $Al_{20}H_{60}$. This suggests that bulk alane (which is approximated by the large cluster) is unstable. In contrast, desorption energies of 0.4–0.6 eV/H_2 are observed for Al_8H_{24} to $Al_{16}H_{48}$; these are desirable for hydrogen storage applications [21]. Further research into alane and other binary metal hydrides is on-going.

3.1.1.2. Intermetallic hydrides. Intermetallic hydrides are hydrides that contain at least two metals in addition to hydrogen. They were the first hydrides investigated because they can adsorb and desorb hydrogen under mild conditions. This is very important because many hydrogen storage materials do not work in the narrow range available in fuel cell vehicles (1–10 atm, 298–393 K). Fig. 8 shows the equilibrium pressure–temperature curves for several metal hydrides with the ideal P–T operating window outlined with a dark black square. As can be seen, only a few metal hydrides work in this range, all of which are intermetallic [8].

Although several intermetallic hydrides operate in the desired range, most have a gravimetric capacity too low and cost too high for vehicular applications. As a result, $LaNi_5H_6$ (Fig. 9a) is one of the few that is currently commercially available. In order to find other potential hydrides and knowing the many advantageous properties of alane (Section 3.1.1.1), intermetallic hydrides that include an alane group have been extensively researched. One of the most common is sodium alanate (Fig. 9b), which releases hydrogen through reactions (R1) and (R2). (R1) releases 3.7 wt% hydrogen at 1 atm and 306 K; (R2) releases 1.8 wt% hydrogen at temperatures above 383 K [8].

$$NaAlH_4 \rightarrow \frac{1}{3}Na_3AlH_6 + \frac{2}{3}Al + H_2 \quad \text{(R1)}$$

$$Na_3AlH_6 \rightarrow 3NaH + Al + \frac{3}{2}H_2 \quad \text{(R2)}$$

The theoretical maximum material gravimetric capacity of sodium alanate is 5.5 wt% hydrogen, which is slightly below the DOE 2010 target of 6 wt%. Unfortunately, the hydrogen release kinetics are quite slow and the packing density of the powder is low (ca. 50% of the theoretical crystal density), which makes the system volumetric capacity quite low. Therefore, sodium alanate is not expected to ever be capable of reaching the DOE targets [8].

Table 1 – Volumetric and gravimetric hydrogen content in mechanical storage systems and metal hydrides.

Storage method or material	Number of hydrogen atoms per cm^3 ($\times 10^{22}$)	Wt% hydrogen
H_2 gas (197 atm)	0.99	100
H_2 liquid (20 K)	4.2	100
H_2 solid (4 K)	5.3	100
MgH_2	6.5	7.6
Mg_2NiH_4	5.9	3.6
$FeTiH_{1.95}$	6.0	1.89
$LaNi_5H_{6.7}$	5.5	1.37
$ZrMn_2H_{3.6}$	6.0	1.75
VH_2	11.4	2.10

Reprinted from Ref. [22] with permission.

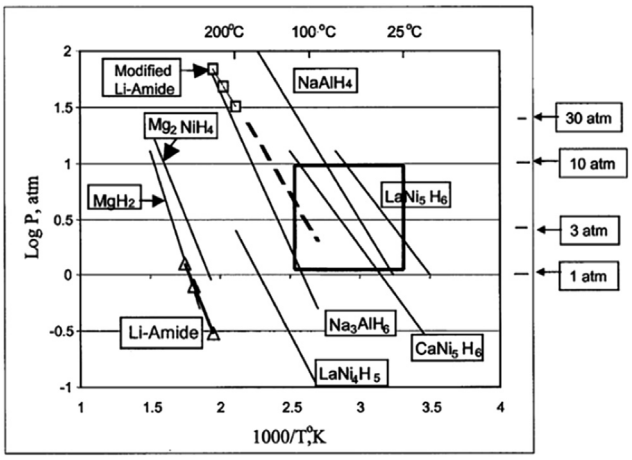

Fig. 8 – Equilibrium pressure–temperature curves for simple metal hydrides; operating conditions for fuel cell vehicles are highlighted in a black box. Reprinted from Ref. [8] with permission.

Newer intermetallic hydrides contain more than two metals, often transition metals, with non-stoichiometric compositions. These materials are not yet fully investigated, but they are hoped to have higher hydrogen discharge capacities than the simpler hydrides. This has been found to be true for several compounds, such as $La_{0.7}Mg_{0.3}Ni_{2.8}Co_{0.5}$, which has a hydride discharge capacity of 410 mA/g compared to 320 mA/g for a typical AB_5-type hydride. Other structures under investigation include $Ti_{0.32}Cr_{0.32}V_{0.25}Fe_{0.03}Mn_{0.08}$, $MmNi_{4.6}Fe_{0.4}$ and many more. While these hydrides have many promising properties, their high metal concentration limits the gravimetric capacity to 3 wt% H_2. As a result, they are not currently commercially viable [25–27].

3.1.2. *Complex metal hydrides*

Complex metal hydrides contain hydrogen atoms that are partially covalently bound within a polyatomic anion. They often have higher gravimetric capacities than simple hydrides. There are two main categories of complex hydrides: nitrogen-containing hydrides (amides or imides) and boron-containing hydrides (borohydrides). These are usually bound to lithium or magnesium, but can also be associated with sodium, calcium or, less commonly, transition metals. Multiple compounds can be combined to make systems with enhanced properties. Due to the large volume of complex metal hydrides, only the most common are discussed in this paper [8,23].

3.1.2.1. Amides and imides. The most common cation paired with amides and imides is lithium. Lithium imide, Li_2NH (Fig. 10a), adsorbs hydrogen in reaction (R3) at 1 atm and 558 K.

$$Li_2NH + H_2 \leftrightarrow LiNH_2 + LiH \quad (R3)$$

This reaction reversibly stores 6.5 wt% hydrogen, which is promising, but the required temperature is outside the operating range of FCVs. Therefore, Li_2NH use would require heat to be generated on board, likely by burning the fuel. This would increase the system cost, volume and weight and decrease efficiency. Magnesium amide, $Mg(NH_2)_2$ (Fig. 10b), was considered as an alternative because it has a more efficient dehydration reaction and is stable at a temperature of only 473 K. However, it also has a slight reduction in hydrogen capacity. Therefore, nitrogen-containing metal hydrides do not seem promising [8].

Even if an amide was found that produces enough hydrogen at a reasonable temperature, amides and imides will always be problematic because ammonia is formed as a by-product during hydrogen release. Since ammonia is a poison for PEM fuel cells, it cannot be present at concentrations greater than 0.1 ppm [8].

3.1.2.2. Borohydrides. The most common borohydrides are lithium borohydride, $LiBH_4$ (Fig. 11a), and sodium borohydride, $NaBH_4$ (Fig. 11b). They are promising materials because they have very high potential hydrogen contents of up to 18 wt%. Unfortunately, use of $LiBH_4$ and $NaBH_4$ is currently limited because temperatures greater than 673 K are required for dehydrogenation (reaction (R4)). Substantial effort has gone into finding ways of thermodynamically destabilizing the materials [30].

$$\frac{2}{3}LiBH_4 \leftrightarrow \frac{2}{3}LiH + \frac{2}{3}B + H_2 \quad (R4)$$

Several destabilization techniques were investigated. The first is incorporation of additives to the fuel mixture. These

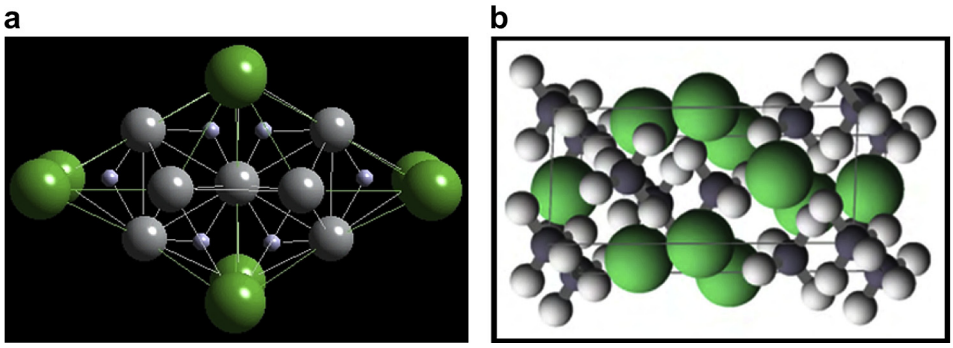

Fig. 9 – Crystal structure of $LaNi_5H_6$ where La = green, Ni = grey, H = white (left, a) and sodium alanate where Na = green, Al = grey, H = white (right, b). (For interpretation of the references to colour in this figure legend, the reader is referred to the web version of this article.) Reprinted from Refs. [23(a), 24(b)] with permission.

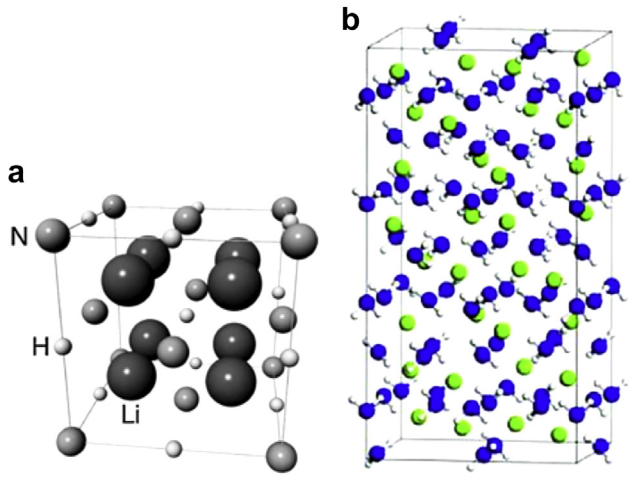

Fig. 10 – Crystal structure of lithium imide where Li = black, N = grey, H = white (left, a) and magnesium amide (right, b) where Mg = blue, N = green, H = white. (For interpretation of the references to colour in this figure legend, the reader is referred to the web version of this article.) Reprinted from Refs. [28(a), 29(b)] with permission.

include pure metals, metal oxides or halides, lithium amide, sulphides, other hydrides (Section 3.1.2.3) or nanoporous scaffolds. The second option is to change the cation. Both techniques show promise. A recent study investigating the effect of changing the cation found that dehydrogenation temperature decreases as cation electronegativity increases. A study into the effect of metal doping found that if $NaBH_4$ is doped with titanium, B–Ti bonds form. These destabilize the borohydride cage and cause an increase in mobility of the hydrogen atoms [23,30].

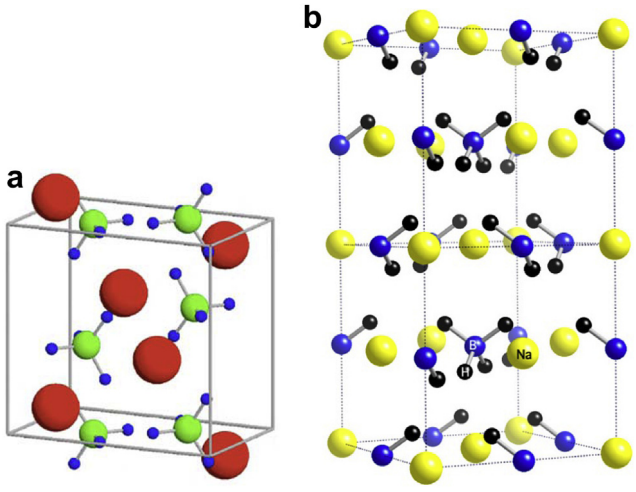

Fig. 11 – Crystal structure of lithium borohydride at room temperature where Li = red, B = green, H = blue (left, a) and sodium borohydride where Na = yellow, B = blue, H = black (right, b). (For interpretation of the references to colour in this figure legend, the reader is referred to the web version of this article.) Reprinted from Refs. [31(a), 32(b)] with permission.

A final option to decrease the hydrogen release temperature of borohydrides is to change the mechanism by which hydrogen is released. The technique used for this is hydrolysis, or reaction with water. Sodium borohydride is more commonly used for this because its reaction is safer than that of the lithium equivalent. $NaBH_4$ reacts with water spontaneously to produce hydrogen at room temperature by reaction (R5). This reaction takes 2.5 or 16 min with a platinum or fluorinated cobalt catalyst respectively. These conditions are desirable and so this reaction would be very promising except that it is not reversible. Therefore, it can only be implemented in one-time use applications [30].

$$NaBH_4 + 2H_2O \rightarrow NaBO_2 + 4H_2 \quad \text{(R5)}$$

3.1.2.3. *Combination systems*. As was mentioned in the previous section, useful materials can be created by combining two hydrides that have individual limitations. This was done, for example, with lithium borohydride, $LiBH_4$ destabilized with magnesium hydride, MgH_2. Lone $LiBH_4$ produces hydrogen by reaction (R4). However, when MgH_2 is added, hydrogen is generated by reactions (R6) and (R7) with (R6) acting as an intermediate reaction that occurs at lower temperature [8].

$$\frac{1}{2}LiBH_4 + \frac{1}{4}MgH_2 \leftrightarrow \frac{1}{2}LiH + \frac{1}{4}MgB_2 + H_2 \quad \text{(R6)}$$

$$\frac{1}{2}LiBH_4 + \frac{1}{4}MgH_2 \leftrightarrow \frac{1}{2}LiH + \frac{1}{2}B + \frac{1}{4}Mg + H_2 \quad \text{(R7)}$$

The formation of dehydrogenated MgB_2 can reduce the temperature for hydrogen release by ca. 240 K compared to pure $LiBH_4$. Unfortunately, dehydration still requires a temperature of 648 K and has slow kinetics. One method to improve this involves nanoengineering to make smaller material particles (Fig. 12). This will decrease the hydrogen diffusion distance, which in turn will increase the hydrogen exchange rate [8].

3.2. *Non-metal hydrides*

Historically, non-metal hydrides have been less common than metal hydrides because metals are known to bind hydrogen more strongly than non-metals. However, the large weight associated with metals has made non-metal hydrides increasingly popular in recent years. Non-metal hydrides contain boron, carbon, nitrogen or oxygen in addition to hydrogen. These elements are among the most reactive non-metals and can interact well with hydrogen because they are also quite small.

3.2.1. *Hydrocarbons*

Of non-metal hydrides, hydrocarbons have been the most extensively investigated because their use would require minimal changes to the current energy infrastructure. Hydrogen can be produced from both gaseous (C_1–C_3) and liquid (C_4–C_{10}) hydrocarbons. Unfortunately, hydrogen generation from hydrocarbons is not easy and often produces byproducts that poison the fuel cell, such as sulphur gas or carbon monoxide [33].

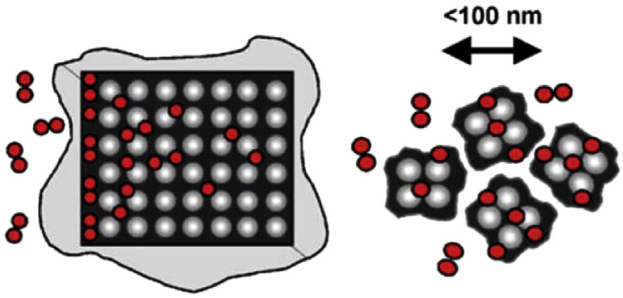

Fig. 12 – Increased hydrogen diffusion in nanoscale destabilized $LiBH_4$ material. Reprinted from Ref. [8] with permission.

There are several methods available to extract hydrogen from hydrocarbons. These include steam reforming (SR), partial oxidation reforming (POX) and autothermal reforming (ATR). SR has the highest efficiency but it is an endothermic reaction and so is not frequently used. POX is an exothermic reaction, but it must be performed at very high temperatures (>773 K), which makes it unsuitable for on board hydrogen generation [33,34].

Autothermal reforming should be an ideal compromise between SR and POX because ATR combines the other two systems to produce a stand-alone process in which the entire hydrogen generation reaction occurs in one reactor where the heat from POX is used to drive SR. However, this system requires a large area and so is not possible for on board applications. In addition, all reforming reactions require a catalyst that must be chosen based on weight, size, activity, cost, transient operations, versatility to reform different fuel compositions, durability and efficiency [33].

In addition to the aforementioned issues regarding fuel reforming, one of main reasons for using hydrogen fuel is to stop the use of hydrocarbons. Although using H_2 generated from hydrocarbons is more efficient than burning hydrocarbons directly, this is unlikely to be a long-term solution.

3.2.2. *Boron and nitrogen hydrides*

Given the environmental concerns associated with hydrocarbons, boron and nitrogen hydrides have been given a lot of attention. The most common of these are NH_3BH_3 as a borohydride and NH_3 and N_2H_4 as nitrohydrides. Both boron and nitrogen hydrides have very high hydrogen contents. Ammonia borane, NH_3BH_3, has a hydrogen capacity of 19.6 wt%, which is greater than that of petrol; hydrazine, N_2H_4, is a close second with a hydrogen content of 12.6 wt% [30].

Despite their high hydrogen contents, the use of these materials is limited because of the slow kinetics and unfavourable thermodynamics associated with hydrogen release. Therefore, compounds and reactions with the most favourable hydrogen production are currently being investigated [30].

3.2.2.1. Boron-containing hydrides. Ammonia borane, NH_3BH_3, is a very promising compound because of its high hydrogen capacity of 19.6 wt%. However, it does not release H_2 until thermal decomposition. This occurs over several reactions (R8)–(R11) and requires a temperature of ca. 473 K. This temperature can be lowered in organic solutions or ionic liquids with the addition of an acid or transition metal catalyst. Loading the compound into mesoporous silica can also be effective. Unfortunately, NH_3BH_3 dehydrogenation releases unwanted borazine by-products under any conditions [30,35].

$$NH_3BH_3 \xrightarrow{363-393\ K} \frac{1}{x}(NH_2BH_2)_x + H_2 \quad \text{(R8)}$$

$$\frac{1}{x}(NH_2BH_2) \xrightarrow{\sim 423\ K} \frac{1}{x}(NHBH)_x + H_2 \quad \text{(R9)}$$

$$\frac{1}{x}(NHBH)_x \xrightarrow{>423\ K} \frac{1}{x}(NBH)_x + \frac{1}{2}H_2 \quad \text{(R10)}$$

$$\frac{1}{x}(NHBH) \xrightarrow{>773\ K} \frac{1}{x}(NB)_x + H_2 \quad \text{(R11)}$$

Several methods have been found to prevent borazine production during NH_3BH_3 use. One option is to react ammonia borane with metals to produce metal amidoboranes, such as $LiNH_2BH_3$. This material releases 11 wt% hydrogen more cleanly than NH_3BH_3 and at a temperature of only 368 K. Borazine-free hydrogen generation from NH_3BH_3 can also be accomplished by hydrolysis or alcoholysis (reaction with water or alcohol respectively). These reactions occur by (R12) and (R13) respectively. They are cleaner than simple dehydrogenation and occur much faster [30].

$$NH_3BH_3 + 2H_2O \rightarrow NH_4BO_2 + 3H_2 \quad \text{(R12)}$$

$$5NH_3BH_3 + 22CH_3OH \rightarrow \left[NH_4B(OCH_3)_4\right]_5 \cdot CH_3OH + 15H_2 \quad \text{(R13)}$$

Hydrogen release from all compounds discussed in this section and Section 3.1.2.2 is shown in Fig. 13 where the gravimetric hydrogen capacity is calculated by the total weight of the storage material plus the weight of the reactants. From this data, NH_3BH_3 produces the most hydrogen at the lowest temperature, followed closely by $NaBH_4$, with $LiBH_4$ being the least favourable storage material [30].

3.2.2.2. Nitrogen-containing hydrides. Ammonia, NH_3, is the most promising nitrohydride for two reasons. First, it has the highest hydrogen content of all the nitrohydrides at 17.7 wt%. Second, ammonia production technology already exists. Therefore, ammonia use would cause minimal disruption to current infrastructure [30].

Hydrogen is obtained from ammonia decomposition in reaction (R14). This reaction is endothermic so a high temperature is required to obtain significant amounts of H_2. Catalysts, most notably ruthenium, can increase the reaction efficiency, but the temperatures required are still too high for general use. An alternative mechanism involves combining ammonia with lithium hydride to produce hydrogen and lithium amide in reaction (R15). By this reaction, 8.1 wt% hydrogen can be generated at room temperature. In addition, (R15) is reversible and lithium amide can store another 8.1 wt% hydrogen at high temperature and pressure. Therefore, this reaction has real promise for fuel cell vehicles [30,36].

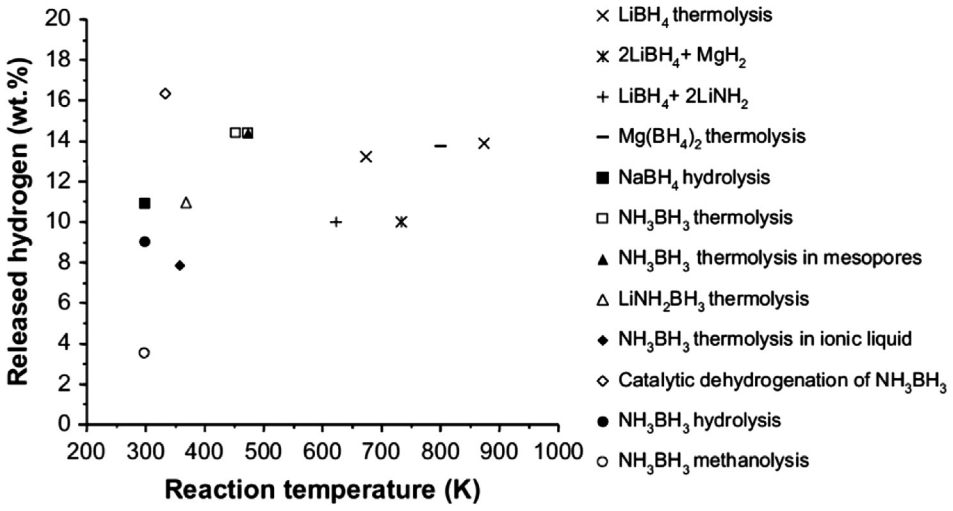

Fig. 13 – Hydrogen release from boron-containing materials. Multiple points are given for the same system when two references yielded unique results. Reprinted from Ref. [30] with permission.

$$2NH_3 \rightarrow N_2 + 3H_2 \quad \text{(R14)}$$

$$NH_3 + LiH \leftrightarrow LiNH_2 + H_2 \quad \text{(R15)}$$

Another potentially useful nitrohydride is hydrazine, N_2H_4, which has a hydrogen content of 12.6 wt%. Hydrazine can be hard to work with because it is hypergolic, which means that it reacts explosively when brought into contact with oxidizing agents. However, once diluted in water or an inert gas, hydrazine is quite stable [30].

Hydrazine decomposition occurs via reaction (R16) at 523 K. This reaction is not useful because it produces NH_3 instead of H_2. Hydrogen cannot then simply be generated from the produced ammonia because there is competition between reactions (R14) and (R16). However, at higher temperatures or in the presence of a catalyst, such as supported-Ni, Pt, Pd or Ir, hydrogen can be produced from hydrazine directly in reaction (R17) [30].

$$3N_2H_4 \rightarrow 4NH_3 + N_2 \quad \text{(R16)}$$

$$N_2H_4 \rightarrow 2H_2 + N_2 \quad \text{(R17)}$$

Hydrogen release from all compounds discussed in this section and Section 3.1.2.1 are shown in Fig. 14 where the released hydrogen is calculated by the total weight of the chemical hydrogen storage material plus the weight of reactants. From this data, hydrazine and an ammonium–lithium amide mixture are the most promising nitrogen-containing compounds; amides do not hold enough hydrogen and ammonia requires unrealistically high operating temperatures [30].

4. Adsorption materials

The final method of hydrogen storage discussed in the present paper is adsorption to porous materials. This includes metal organic frameworks (Section 4.1), carbon and other nanostructures (Section 4.2) and the far less common clathrates (Section 4.3).

In order for adsorption materials to be effective, they must have high surface areas and so are usually very porous. This concept is demonstrated by calculations using Fig. 15. First, the surface area of a pure graphene sheet (Fig. 15a) is calculated. Next, smaller areas of the surface are removed and the surface area re-calculated. When the full sheet is cut so that it contains separated rows of benzene rings (Fig. 15b), the latent edges of the rings become exposed, causing the surface area to increase from 2965 to 5683 m^2/g. Alternatively, if the sheet is divided into groups of four rings (Fig. 15c), the surface area is slightly larger at 6200 m^2/g. Finally, the sheet is reduced to single benzene rings (Fig. 15d). This exposes all latent edges and produces the upper limit of possible exposed surface area as 7745 m^2/g. Although this value can never be realistically obtained, it indicates that structures with a lot of exposed rings have very high surface areas and so are the most useful for hydrogen storage. This same concept applies to non-carbon materials [37].

4.1. *Metal organic frameworks*

Metal organic frameworks (MOFs) are crystalline solids composed of metal ions or clusters connected by molecular bridges. They contain nanometre cavities between the metal atoms, which can be filled with gas particles. Prior to MOFs, the largest surface area observed in structural supports was 2030 m^2/g in disordered carbon; MOFs typically have surface areas greater than 3000 m^2/g [37,38].

One of the first high surface area MOFs to be synthesized was Zn_4O(1,3,5-benzenetribenzoate)$_2$ or MOF-177 (Fig. 16a, b) in 2003. It has a surface area of 4500 m^2/g when measured by N_2 at 77 K. When hydrogen is used, MOF-177 does not reach saturation at atmospheric pressure and H_2 adsorbs less strongly than N_2. This suggests that pore-filling is not possible at reasonable pressures. Therefore, if MOF-177 is to become commercially viable, the pore size must be optimized to

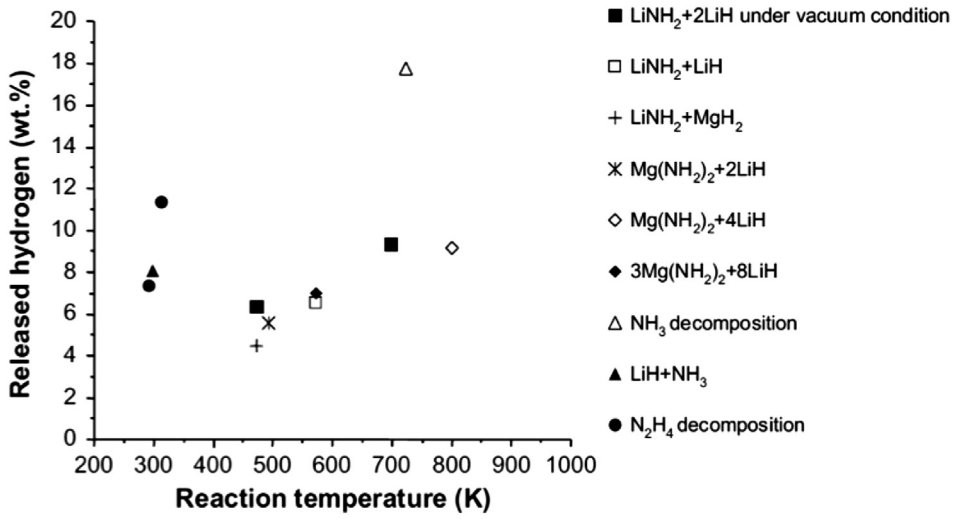

Fig. 14 – Hydrogen release from nitrogen-containing hydrides. Multiple points are given for the same system when two references yielded unique results. Reprinted from Ref. [30] with permission.

reduce the fraction of under-utilized space; this will in turn increase the volumetric capacity of the material [38].

The ideal pore size (shown as a yellow sphere in Fig. 16) for maximum attraction of adsorbate to the MOF is the same as the adsorbate's van der Waal diameter. Ideal pores require thin walls and so should be composed of light elements, one atom thick and highly segmented. This requires short linking groups between metal atoms. This is problematic because it increases the gravimetric density of the material [38].

Another approach to increase the contactable surface area within large pores is to insert another adsorbate molecule by impregnating the MOF with a non-volatile guest. A guest reduces the diameter of the pores and provides additional adsorption sites. An impregnation species must be chosen carefully so that it does not add significant weight or block existing adsorptive sites. In addition, the guest must have low vapour pressure so that it is not desorbed during removal of hydrogen. A reactive species would be ideal to increase attraction of hydrogen to the MOF, but this is not always possible. Buckminsterfullerene, C_{60}, and Reichardt's dye have been shown to incorporate well into MOF-177 (Fig. 17). This is shown with C_{60} in Fig. 16c [38].

A third option to decrease pore size in MOFs is catenation with another identical framework. This can be done by interpenetration, in which the frameworks are maximally displaced from each other (Fig. 18a), interweaving, where there is minimal displacement (Fig. 18b), or a combination of the two (Fig. 18c) [38].

The combination technique is most common because the individual techniques have both advantages and disadvantages. Interpenetration is more effective at maximizing exposed surfaces than interweaving because it decreases pore size without blocking adsorptive sites. Unfortunately, interpenetrated states are often unstable when the MOF is evacuated. In contrast, interweaving reinforces the individual frameworks and so improves the rigidity and stability of the MOF in the absence of hydrogen. However, this also causes thickening of the walls, which reduces the number of adsorptive sites [38].

One way to increase the effectiveness of catenation is to create open metal sites, which strengthens H_2 physisorption. This can be done by removing the axial ligands from the inserted MOF (Fig. 19). This is possible if the ligand is weakly bound to the metal and if the MOF maintains its shape after the ligand is removed. Alternatively, open metal sites can be created by embedding them within the linker. Removal of the axial ligands is often favoured because it also decreases the density of the framework [38].

Catenation has been shown to be effective in a study that compared MOF-177 (Fig. 18) and IRMOF-1, 8, 11 and 18 (Fig. 20).

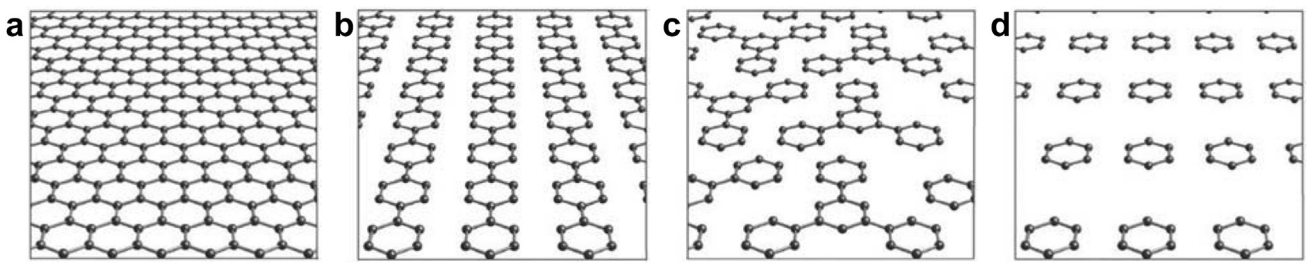

Fig. 15 – Surface area of graphene fragments used to calculate the theoretical upper limit of possible surface area. Reprinted from Ref. [37] with permission.

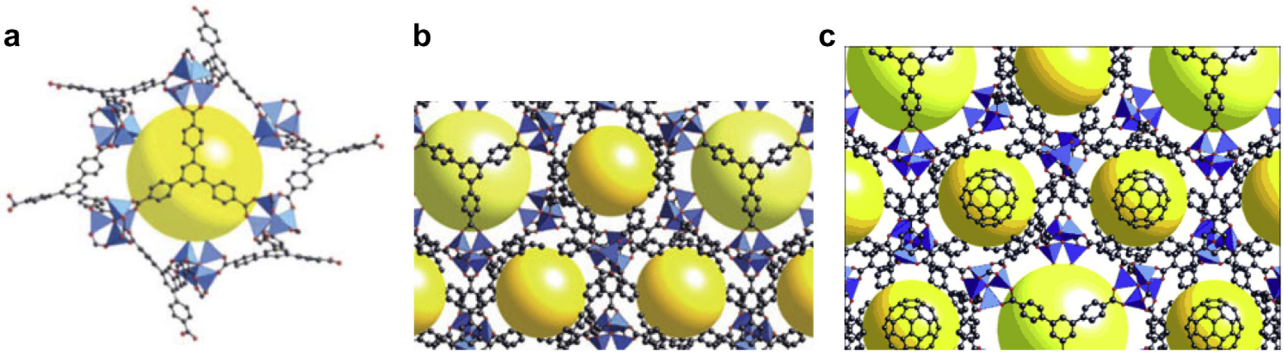

Fig. 16 – Crystal structure of MOF-177 with C = black, O = red, Zn = blue polyhedral; yellow spheres contact the van der Waals radii of the framework atoms to indicate the pore volume. It is displayed as a single molecule (a), in a molecular group (b) and impregnated with C_{60} (c). (For interpretation of the references to colour in this figure legend, the reader is referred to the web version of this article.) Reprinted from Ref. [38] with permission.

Although previous studies found that hydrogen had the strongest interaction in IRMOF-1, a study involving catenation showed that fourfold interwoven IRMOF-11 has the strongest hydrogen uptake; it was able to absorb 1 wt% hydrogen at room temperature and 47 atm [39].

Another important aspect to consider is the influence of different metals. An effective metal must have good attraction to hydrogen and not add significant weight to the system. Zinc is most commonly used, but light main group elements, such as Li, Na, Mg and Al, have more desirable weights. Unfortunately, the main group monovalent cations are impractical because they make the MOF susceptible to hydrolysis; main group multivalent cations have strong polarizing power that should be useful for producing strong coordination bonds, but they form oxides easily. For example, an aluminium MOF, MIL-53 synthesized in the mid-2000's, had a good hydrogen adsorption capacity of 3.8 wt% at 77 K and 15.8 atm, but it showed usually high hysteresis upon desorption and so could not be used [38].

In addition to these main group elements, other transition metals have been considered as well. For example, recent work investigated the hydrogen storage capacity in iron MOFs and found that a theoretical reversible hydrogen storage of 6.0 wt% was achieved at 298 K and 100 atm. Heterometallic MOFs have also been studied. One example of a cerium–zinc MOF, $Ce(oda)_3Zn_{1.5}(H_2O)_3{\cdot}0.75H_2O$, shows an experimental reversible hydrogen storage of 1.34 wt% at 77 K and 0.86 wt% at 298 K and 33.5 atm [41,42].

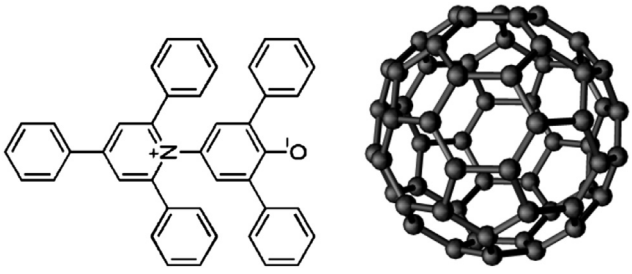

Fig. 17 – Structure of Reichardt's dye (left) and buckminsterfullerene (right).

4.2. *Nanostructures*

4.2.1. *Carbon materials*

Hydrogen adsorption on carbon nanomaterials is a relatively new field because these structures have only been available in the last few decades. Initial work began with carbon nanotubes (CNTs, Section 4.2.1.2) in the late 1990's. Since then, hydrogen adsorption on several different fullerenes and activated carbons has been studied [43].

Fig. 21 shows gravimetric hydrogen storage capacities on many carbon nanofibres (Fig. 21a), nanotubes (Fig. 21b) and activated carbons (Fig. 21c). The highest values occur on carbon nanofibres with 67.55 wt% on herringbone graphite nanofibres and 53.68 wt% on platelet graphite nanofibres at room temperature and 110 atm. The highest values for nanotubes are 20 wt% for Li-doped CNTs and 14 wt% from K-doped systems. No general trends are observed on either carbon nanofibres or nanotubes and the extreme results are not reproducible. In contrast, for activated carbons, a reproducible general trend shows that hydrogen adsorption increases with decreasing temperature and increasing pressure. However, the highest hydrogen storage is only 5 wt% on AC-21 at 77 K and 30–60 atm [43].

4.2.1.1. *Activated carbon.* Activated carbons were one of the first carbon materials considered for hydrogen storage. Although, they cannot hold as much H_2 as other carbon materials, they are desirable because they can be easily produced and their chemistry is relatively well understood [43].

In general, the gravimetric hydrogen capacity of activated carbons is correlated with the amount and distribution of porosity in the material. A high micropore volume and narrow size range leads to the highest hydrogen uptake. However, at lower temperatures the material becomes more absorbent so the micropore size distribution is less important [43].

One of the most effective activated carbons is KUA5. At room temperature, it absorbs 3.2 wt% hydrogen at 187 atm and 6.8 wt% at 493 atm; at 77 K, it absorbs 8 wt% at only 39 atm. This suggests that activated carbons can be effective for hydrogen storage, but only at low temperatures. However, a recent study of another activated carbon, AX-21, found that

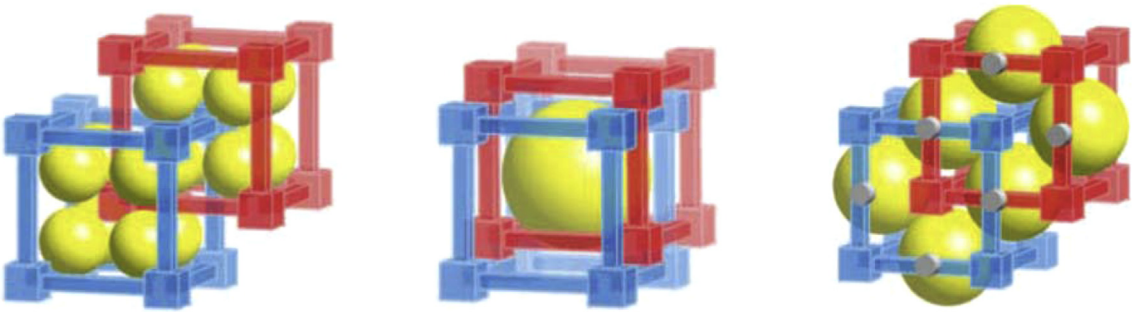

Fig. 18 – Schematic representation of MOFs depicted as cubes and rods showing catenation by interpenetration (left), interweaving (centre) and a combination (right) where the yellow sphere indicates the pore volume. (For interpretation of the references to colour in this figure legend, the reader is referred to the web version of this article.) Reprinted from Ref. [38] with permission.

even cryogenic storage is difficult. AX-21 was previously shown to have a relatively high hydrogen storage capacity of 5.4 wt% at 77 K, but the recent cryogenic study found that at 100 K, it does not enhance the hydrogen storage capacity above that of the non-adsorbed cryocompressed gas. In addition, more than 80% of the sorption capacity is irrecoverable at 99 atm and 100 K. Finally, 11 kWh of electricity are required per kilogram of dispensed H_2 if off-board liquid N_2 is used to cool the gas. Therefore, refuelling is energy-expensive [43,46].

Cryogenic storage is also difficult because the tank must be cooled. This can be accomplished by surrounding it with vacuum insulation and having minimal conduction paths to the ambient atmosphere. This increases the volume and cost of the system. In addition, the small amount of heat generated when hydrogen adsorbs to the carbon surface must be removed when the tank is refuelled. Heat transfer is difficult for any cryogenic systems and is especially difficult for cryo-adsorption because activated carbons have low thermal conductivity. Finally, a temperature swing is usually required to desorb the H_2 gas, which makes the system design more complicated, larger and more costly [44].

4.2.1.2. *Carbon nanotubes*. Carbon nanotubes (CNTs) were the first carbon material considered for hydrogen storage in 1997 because they have a microporous structure with high specific surface area. In addition, CNTs can adsorb hydrogen onto the interior and exterior of their nanostructure. This leads to storage capacities of 0.25–11 wt% hydrogen under varying conditions. When metals are added to the systems (Section 4.2.1.4), the gravimetric capacity increases to 1.8 to 20 wt%. The variation in these results can be effected by defects in the CNTs and open versus closed structures [45].

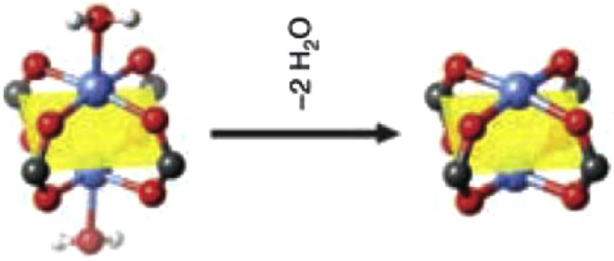

Fig. 19 – Example of removing the axial H_2O ligands from the $Cu^{(II)}$ carboxylate "paddlewheel" cluster MOF. Reprinted from Ref. [38] with permission.

In order to better understand how much H_2 can be held in each class of CNTs, a recent study looked at single-, double- and tripled-walled CNTs and a bundle of single-walled carbon nanotubes (SWCNTs). These classes were then subdivided according to size where the smallest tubes experience fracture in order to meet the DOE targets; medium tubes experience strain; large tubes are not affected; and extra-large tubes self-collapse upon hydrogen release. The chirality and radii of each class of CNTs required to meet the 2010 DOE targets (6 wt% H_2, 62 kg H_2/m^3) are shown in Table 2 [45].

These results suggest that large-sized single- (alone or in a bundle) and double-walled CNTs can meet the DOE hydrogen storage goals. Smaller and larger nanotubes can meet the targets theoretically, but they are damaged in the process and so are not reusable. This is especially true for the small and extra-large nanotubes [45].

A further Monte Carlo study looked into a largely unstudied aspect of carbon nanotubes – packing in 3D covalent assemblies. These are different than the nanotube bundles mentioned in Table 2, in which the CNTs are joined by van der Waals forces. In order to model realistic packed structures, which are likely tangled, a 3-periodic arrangement of nanotubes with three or four different orientations of tube axes were modelled (Fig. 22) [46].

The simulated structures were found to have very high hydrogen uptakes up to 19 wt% at 99 atm and 77 K. These are the highest hydrogen storage capacities observed for non-decorated nanotubes. At room temperature, the storage capacity remained acceptably high at 5.5 wt%. This approaches the 2010 DOE target of 6 wt%. The study also found that hydrogen uptake ability was mainly determined by the nanotube arrangement in space and was almost independent of tube size. Furthermore, H_2 uptake increased proportionally to pore volume at room temperature, but at 77 K, there was an optimal pore size after which hydrogen uptake remained steady [46].

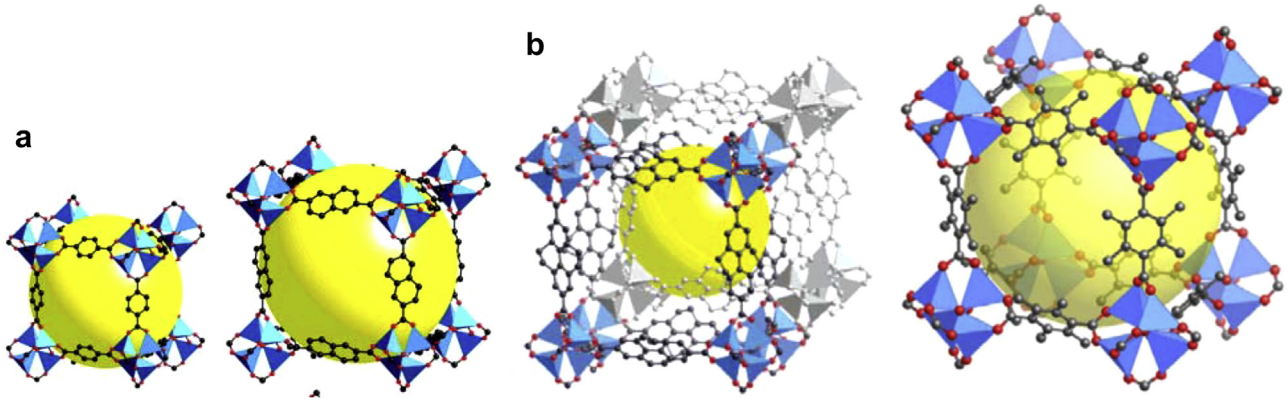

Fig. 20 – Crystal structures of IRMOF-*n* where $n = 1, 8, 11$ and 18 in order of increasing *n* value (left to right) where Zn = blue polyhedral, O = red, C = black and yellow sphere indicates the pore volume. (For interpretation of the references to colour in this figure legend, the reader is referred to the web version of this article.) Reprinted from Refs. [39(a), 40(b)] with permission.

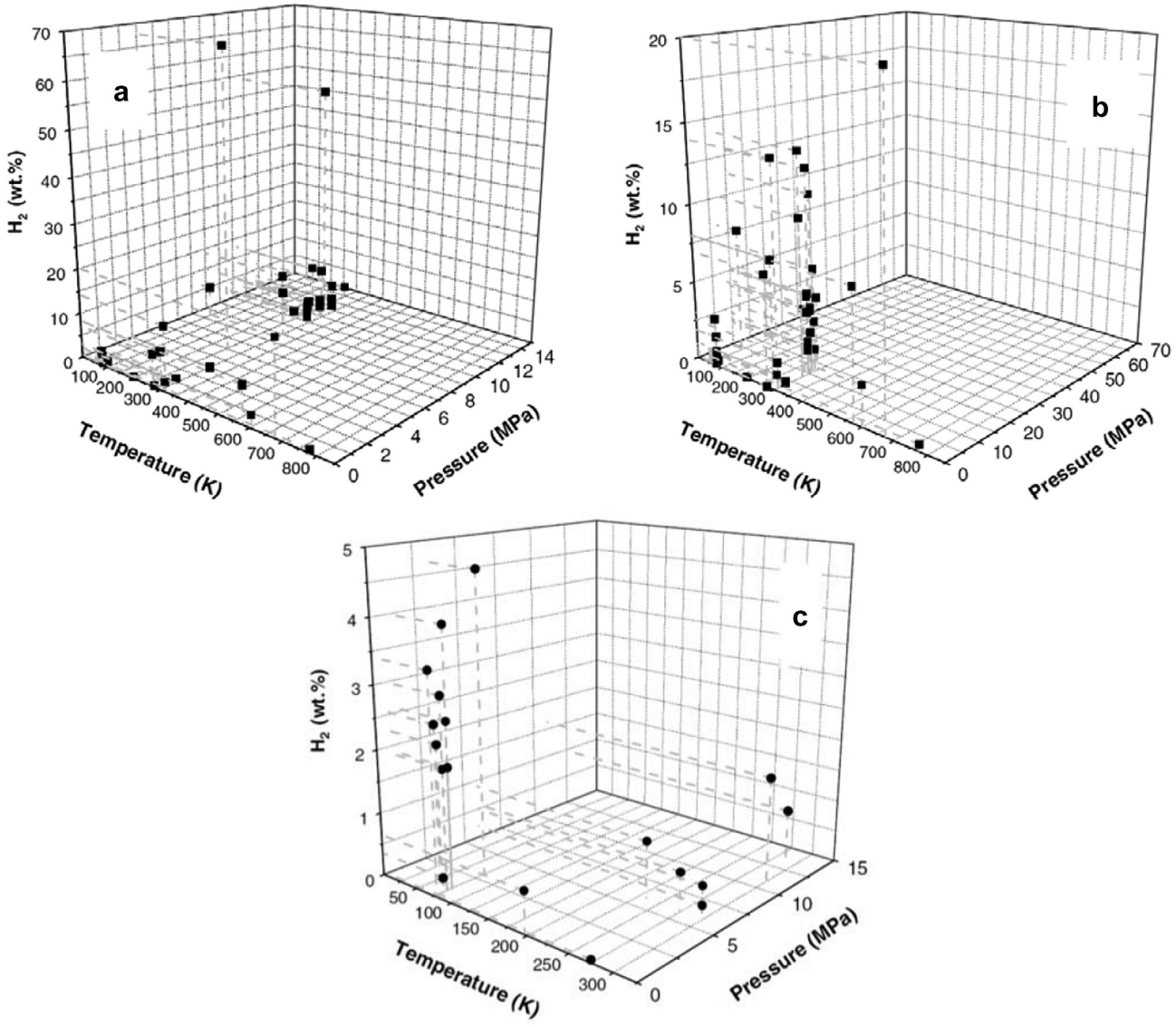

Fig. 21 – Hydrogen storage capacity by weight for carbon nanofibres (top left, a), nanotubes (top right, b) and activated carbons (bottom, c) at several temperature and pressure conditions. Reprinted from Ref. [43] with permission.

Table 2 – Ranges of chirality and radii of several classes of carbon nanotubes required to meet DOE 2010 hydrogen storage targets.

Type of CNT	Reaction to hydrogen release			
	Fracture (small)	Strain (medium)	No effect (large)	Self-collapse (extra large)
Single-walled	(7,7) and down <0.47 nm	(8,8) to (18,18) 0.54–1.2 nm	(19,19) to (30,30) 1.3–2.0 nm	(31,31) and up >2.1 nm
Double-walled	(11,11) and down <0.75 nm	(12,12) to (31,31) 0.81–0.21 nm	(32,32) to (36,36) 2.2–2.4 nm	(37,37) and up >2.5 nm
Triple-walled	(16,16) and down <1.1 nm	(17,17) to (41,41) 1.2–2.8 nm	Not possible	(42,42) and up >2.8 nm
Bundle of SWCNTs	(7,7) and down <0.47 nm	(8,8) to (21,21) 0.54–1.4 nm	(22,22) to (30,30) 1.5–2.0 nm	(31,31) and up >2.1 nm

Reprinted from Ref. [45] with permission.

When the mechanism of hydrogen adsorption was more closely examined at multiple pressures, it was found that at a low pressure of 0.1 atm, adsorption is primarily observed at the sites where the H_2 molecules can simultaneously come close to the surfaces of several nanotubes. This leads to minimal hydrogen accumulation in the centre of the pore (Fig. 23a). As the pressure was increased to 1.0 atm, more H_2 molecules began to cover the external surface of the tubes (Fig. 23b) until they eventually filled the centre of the pore at 99 atm (Fig. 23c) to produce a saturated material [46].

In the case of small tubes, no hydrogen was adsorbed to the interior of the tube; in larger nanotubes, H_2 molecules formed a narrow chain along the tube axis. This suggests that assemblies of larger tubes will have the best storage properties. This research is ongoing [46].

4.2.1.3. *Spherical fullerenes*. The potential hydrogen storage ability of the most common spherical fullerene, buckminsterfullerene, C_{60}, was predicted in 1991 when it was determined that an H_2 molecule can be trapped within a C_{60} cage. Although it is usually unfavourable for hydrogen to be stored in such a space, the high energy barrier required to break the cage open stabilizes the H_2 inside. It was later found that buckminsterfullerene containing one H_2 molecule can be synthesized experimentally with high yield by molecular surgery or by surrounding C_{60} cages with high pressure hydrogen then using laser excitation [47].

Putting larger amounts of H_2 into fullerene cages is currently very experimentally difficult. Therefore, many problems must be answered theoretically before the task can be undertaken. These include how hydrogen is put inside the cage; how H_2 is

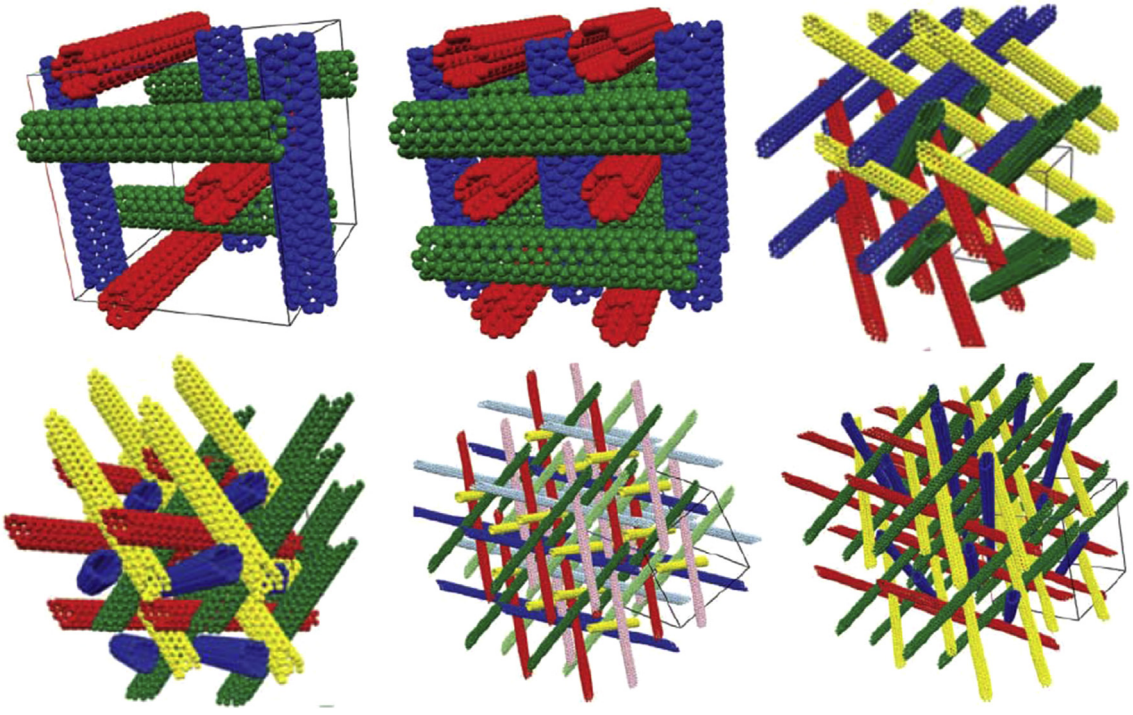

Fig. 22 – Covalent carbon nanotube systems modelled to analyze the effect of packing in 3D covalent assemblies. Reprinted from Ref. [46] with permission.

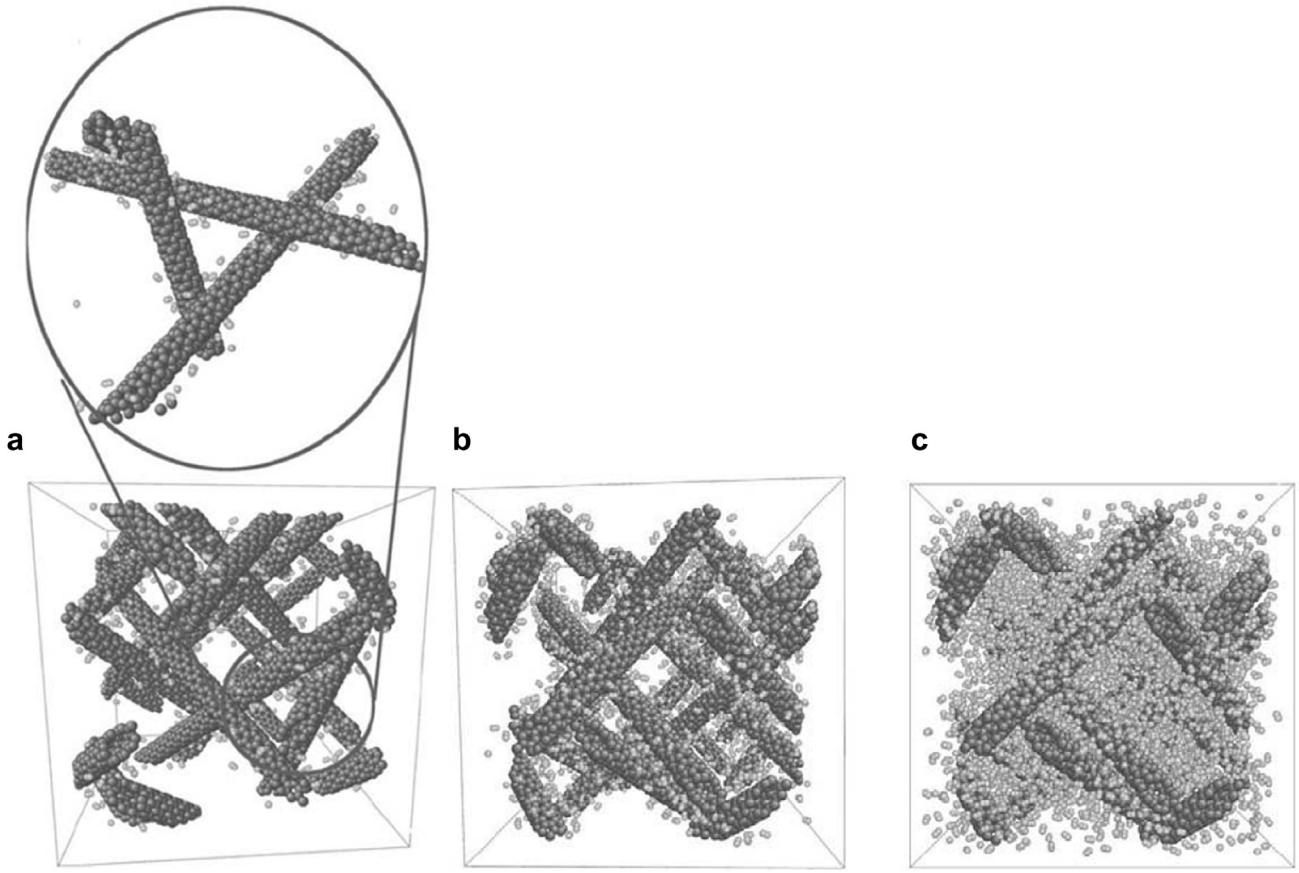

Fig. 23 – Hydrogen adsorption to a packed carbon nanotube assembly at 0.1 atm (left, a), 1 atm (middle, b) and 99 atm (right, c). Reprinted from Ref. [46] with permission.

released and how its release is controlled; and what properties are required for a fullerene to store hydrogen [47].

Buckminsterfullerene is often used as a model compound to investigate these questions. However, there have been disputes as to whether or not C_{60} can realistically store hydrogen. Many scientists claim that only one H_2 molecule will stay in C_{60} because there are high formation energies for complexes containing larger amounts of hydrogen. In contrast, other studies found that 23–25H_2 molecules can be stored within a single C_{60} cage. This often results in fracture of some C–C bonds. On top of this, there is further disagreement about the mechanism of hydrogen storage because it is unknown whether hydrogen atoms chemisorb to the interior surface of the carbon cage or if they exist in the molecular form. As a result, more in depth studies were performed [47].

Further studies found that the formation energies are negative for one or two encapsulated H_2 molecules followed by a value close to zero for three molecules. Buckminsterfullerenes containing four or more H_2 molecules have positive energies of formation and so are metastable. The formation reactions are endothermic and so the complexes are unlikely to form naturally. However, they still correspond to a local minimum of potential energy surfaces until more than 29H_2 molecules are put in the cage. The most densely populated C_{60} cage, containing 29H_2 molecules, has a gravimetric capacity of 7.5 wt%, which exceeds the 2010 DOE target of 6 wt% [47].

When the C–C bond length of buckminsterfullerene was examined for cages containing 1–29H_2 molecules, it was found that the bonds elongate proportionally to the increase in hydrogen molecules, reaching a value of 9.3% increase. This is just below the onset of C–C bond breaking at 11–14.5%. The changes in bond length cause the shape of the fullerene to deviate from spherical (Fig. 24) [47].

When there are less than 10 hydrogen molecules inside the cage (Fig. 24a), all H_2 molecules exist in the molecular form and are organized into well-defined geometric clusters (tetrahedron for four molecules, trigonal bipyramid for five molecules, et cetera). When greater than 10 molecules are placed in the cage, molecular H_2 remains the dominant form of hydrogen, but a few triangular H_3 molecules form as well. This state is likely stabilized by the surrounding polarizable fullerene [47].

When the number of H_2 molecules is further increased to greater than 15 (Fig. 24b), some hydrogen atoms form covalent bonds with the carbon atoms in the fullerene. This is surprising because it is known that chemisorption on a convex carbon surface is much more favourable than on a concave surface because the *p*-orbitals involved in bond formation are mainly localized on the convex surface. However, adsorption on the concave surface is possible because of the high pressure [47].

The length and strength of the C–H bonds are dependent on the amount of encapsulated hydrogen: as the hydrogen

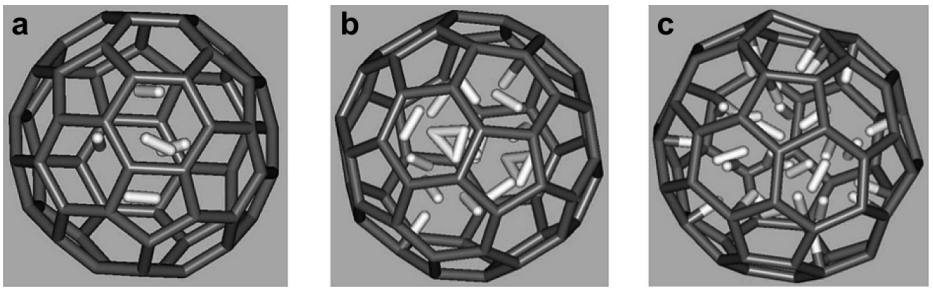

Fig. 24 – C_{60} containing 5 (left, a), 15 (middle, b) and 25 (right, c) H_2 molecules showing the deformation of the fullerene and the formation of H_3 and covalently bound hydrogen. Reprinted from Ref. [47] with permission.

pressure increases, the C–H bond length decreases. However, the bond length increases again when more than $24H_2$ molecules are present in the cage (Fig. 24c) so that $H\cdots H_2$ van der Waals interactions can occur. When C–H bonds are formed, the C_{60} structure becomes deformed in order to produce more sp^3-hybridized carbon atoms that are able to bond hydrogen. This causes the surface to become flattened near the C–H bonds and so the fullerene has increased curvature elsewhere. The sp^3-hybridized carbon atoms no longer contribute to the fullerene's conjugated π-system so the cage is weakened [47].

If more hydrogen is placed in the system, the fullerene will eventually break open. This is initiated by the breaking of a C–C bond involving one carbon that is bound to a hydrogen atom and one that is not. When the non-hydrogenated carbon is completely surrounded by partially hydrogenated carbon atoms, there is nowhere for its *p*-electron density to go. Therefore, one of its C–C bonds breaks, causing the neighbouring carbon to become fully hydrogenated and the initial carbon to become a radical. The hydrogen atoms then shift position to restore the sp^2 character of the carbons while internal pressure pushes the remaining hydrogen towards the opening. Due to the hydrogenation of the terminating carbon atoms, the process is irreversible. This is shown in Fig. 25 with the bond that breaks highlighted in black [47].

Regardless of its uptake and release mechanisms, putting H_2 in a fullerene is still largely unfavourable. Therefore, many methods of fullerenes enhancement have been investigated. One option is to charge the fullerene. This can be done by electrochemical doping, ion/electron impact, laser desorption or chemical doping. Electrochemical doping has been experimentally shown to form fullerene anions and cations in solution with irreversible charges up to ±6; ion/electron bombardment or laser deposition produce fullerene ions in the gas phase; chemical doping has not been extensively studied at this point, but it should produce fullerenes with even higher charges. Chemical doping can be done through substitutional, endohedral or exohedral doping of the fullerene with metal atoms (Section 4.2.1.4) [48].

When density functional theory studies analyzed the storage ability of charged fullerenes, the hydrogen binding energy was found to be favourable at 0.18–0.32 eV. This is within the DOE desired range of 0.2–0.6 eV. Within this range, H_2 can adsorb and desorb under near ambient conditions. The study further found that hydrogen binding is delocalized and so surrounds the entire surface of the charged fullerene. This binding is attributed to polarization of H_2 molecules by the electric field near the fullerene surface [48] (Yoon, 2007).

Charged fullerenes have a potential hydrogen storage capacity of 8.0 wt%. Fullerenes containing an endohedral metal atom did not show a significant enhancement to hydrogen binding but systems containing exohedral metal atoms are quite promising [48]. These are further discussed in Section 4.2.1.4.

4.2.1.4. *Metal-decorated carbons*. One method used to increase the hydrogen storage capacity of carbon materials at ambient conditions is combination with metal. This can be done through physical mixing or chemical doping of the carbon surface. Physical mixing is affected by sample concentration, grinding time and intensity and contacts between

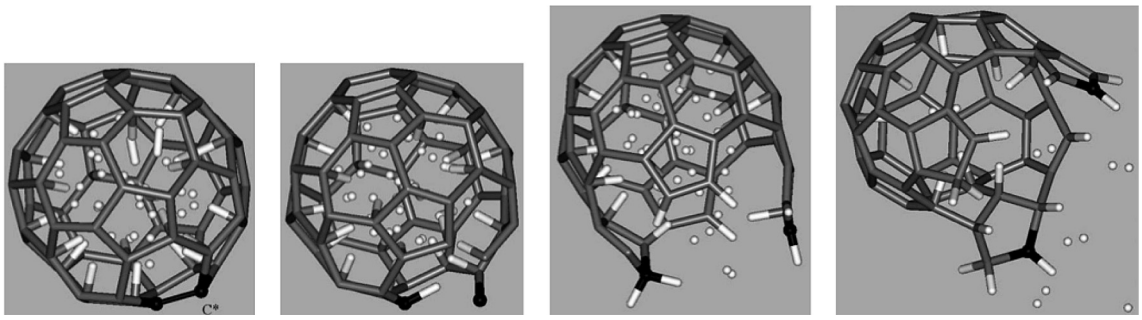

Fig. 25 – Cage opening and hydrogen escape from a C_{60} containing $29H_2$ molecules. The bond that breaks is highlighted in black. Images were obtained by *ab initio* molecular dynamics simulations at 0, 250, 350 and 800 fs respectively. Reprinted from Ref. [47] with permission.

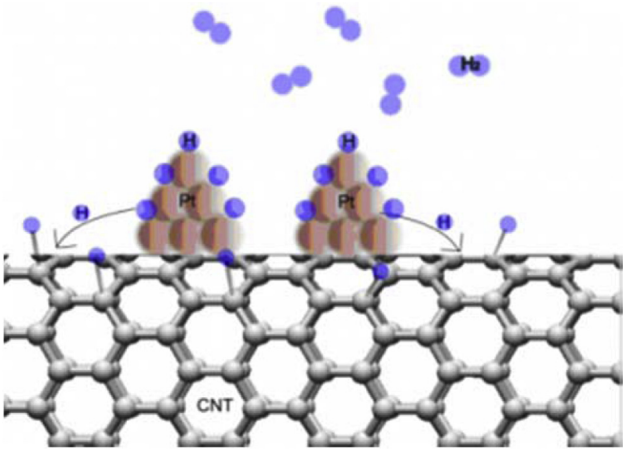

Fig. 26 – Diagram of hydrogen spillover on platinum-decorated carbon nanotubes (CNTs). Reprinted from Ref. [51] with permission.

particles. Therefore, samples are often difficult to reproduce. Chemical doping requires less metal and so is less expensive and more reproducible [49]. It will be the focus of this section.

Carbon decoration with metal nanoparticles has proved very effective in recent years and so is being given considerable attention. One current project investigates hydrogen storage in platinum-decorated fullerenes [50].

Hydrogen storage on metal-decorated carbons occurs by spillover (Fig. 26). Hydrogen spillover is the process of H_2 dissociative chemisorption on metal nanoparticles followed by migration of the hydrogen atoms onto adjacent surface sites [49].

The storage capacity of a metal-decorated carbon material can be enhanced by three factors: (i) identity of the doping metal; this is usually Pt or Pd, although other metals are used; (ii) surface area of the carbon material; (iii) contact between the carbon surface and metal nanoparticles; this is important because large physical and energetic barriers often exist for the transfer of hydrogen atoms from one material to another so close metal–carbon contact is needed [49].

Many studies have looked into optimizing these factors. Since this is a relatively young field, no conclusive results have yet been determined. Therefore, a small sample of studies is provided in this paper as examples of the current research – several different metals and carbon materials are presented through a mixture of experimental and theoretical results. Procedures and mechanisms are not discussed.

One interesting experimental project compared ruthenium, platinum and nickel on templated carbon (TC). It found that Ru is the most effective metal for hydrogen dissociation with the Ru-TC system showing a storage capacity of 1.43 wt% at 298 K and 102 atm. When a direct high-temperature thermal reduction was used to increase contact between Ru and the carbon support, the treated sample had an even higher hydrogen storage capacity of 1.56 wt%. Similar positive results were observed in another study analyzing Pt-decorated AX-21 activated carbon. This study found that the reversible hydrogen storage capacity of 0.6 wt% on AX-21 was increased to 1.2 wt% on Pt/AX-21 at 298 K and 99 atm [49,52].

Similar studies have investigated metal-decorated carbon nanotubes (CNTs). In one such project, first principles calculations found that a single titanium atom adsorbed on the surface of a single-walled carbon nanotube (SWCNT) strongly bond up to four H_2 molecules. This would allow the system to hold 8 wt% hydrogen [53].

Experimental results have not been as favourable. A recent study compared palladium and vanadium-decorated SWCNTs with undecorated treated nanotubes. It found that, although the metal-decorated CNTs showed a higher hydrogen uptake than the untreated nanotubes at room temperature, all systems had very low hydrogen adsorptions of 0.125 wt% on Pd-CNTs and 0.1 wt% on V-CNTs. In a second cycle, only half of the initial hydrogen uptake was obtained. This change was caused by the recrystallization of the defect sites, which are a large source for accepting dissociated hydrogen atoms. In addition, defect recrystallization also caused a decrease in the interaction between the metal and carbon support, which limited the ability for spillover. As a result, hydrogen uptake in the second cycle mostly resulted from H_2 adsorption to the metal surface directly [54].

Metal-decorated spherical fullerenes have also been studied. Recent *ab initio* projects analyzed the effect of C_{60}

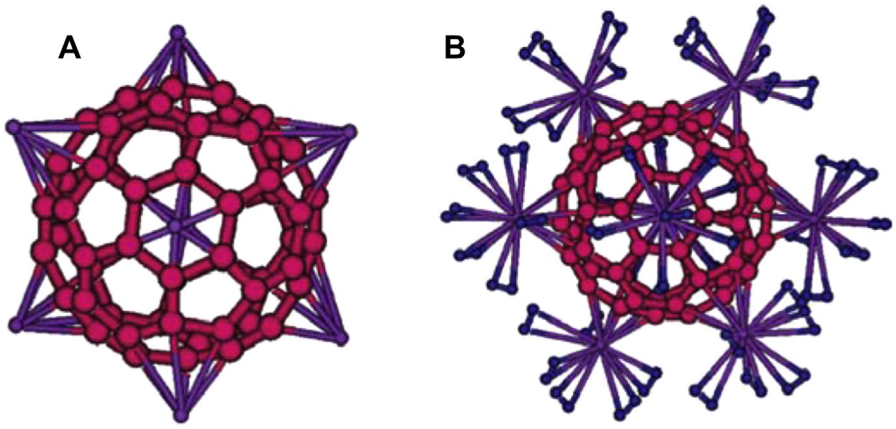

Fig. 27 – C_{60} decorated with eight sodium atoms in the absence (left, A) and presence (right, B) of H_2 molecules. Reprinted from Ref. [55] with permission.

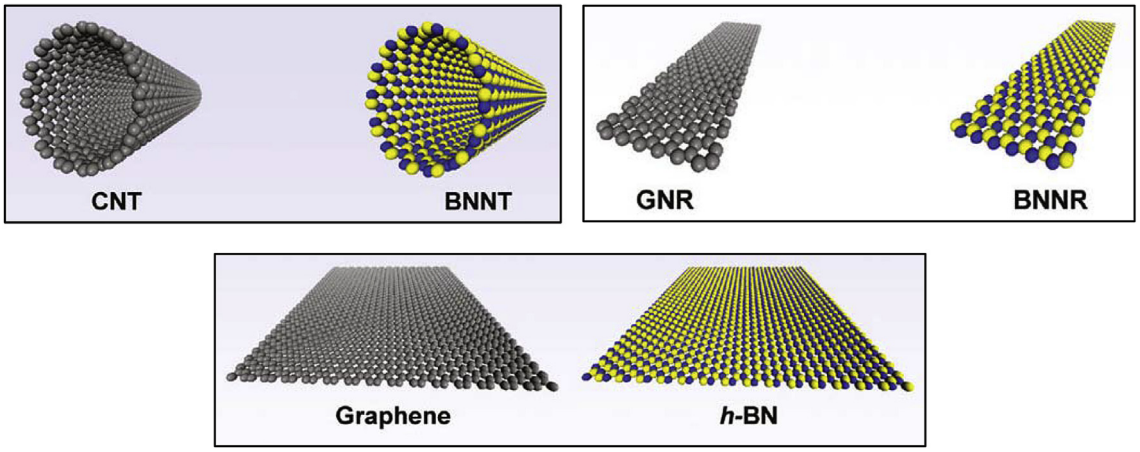

Fig. 28 – Equivalent carbon and boron nitride (BN) nanomaterials where C = grey, B = blue and N = yellow. The carbon structures displayed are a carbon nanotube (CNT) (top left), graphene sheet (bottom) and graphene nanoribbon (GNR) (top right). The BN equivalents are a boron nitrogen nanotube (BNNT), hexagonal boron nitrogen sheet (h-BN) and boron nitrogen nanoribbon (BNNR) respectively. (For interpretation of the references to colour in this figure legend, the reader is referred to the web version of this article.) Reprinted from Ref. [56] with permission.

decoration with alkali metals. These studies found that doping with alkali metals increased the hydrogen adsorption ability of the fullerene by more than traditional transition metals. The most effective system involved sodium where 48 H_2 molecules adsorbed to eight sodium atoms corresponding to a hydrogen storage capacity of 9.5 wt%. This high hydrogen adsorption seems to be a result of ion-molecule electrostatic interactions because it was found that a large number of hydrogen molecules surround the metal ions (Fig. 27). This is a contrast to the hydrogen spillover mechanism observed with transition metals (Fig. 26) [55].

4.2.2. *Other nanostructure materials*

While the focus of hydrogen storage in nanomaterials has centred on carbon materials, there are other nanostructures worth considering. Most of these have a large contribution from boron. Two classes worth mentioning are boron fullerenes, which have identical composition to carbon fullerenes, but are composed of boron atoms instead of carbon atoms, and boron nitride (BN) nanostructures, which have similar geometries to carbon nanostructures, but with alternating boron and nitrogen atoms instead of carbon (Fig. 28). Although the structure of these materials is very similar to that of carbon materials, they can have quite different properties [56,57].

One density functional theory study performed on calcium-decorated boron fullerenes found that the decorating calcium atoms can attract five H_2 molecules each. Given this, the modelled B_{80} system decorated with 12 calcium atoms (Fig. 29a) had a gravimetric density of 8.2 wt% hydrogen with favourable binding energies of 0.12–0.40 eV/H_2. Similarly, a Ca-decorated boron nanotube (Fig. 29b) had a hydrogen storage capacity of 7.6 wt% with binding energies of 0.10–0.30 eV/H_2. Most importantly, adsorption and desorption of these H_2 molecules was favourable at ambient conditions. These results are very promising, but they have not yet been reproduced experimentally [57].

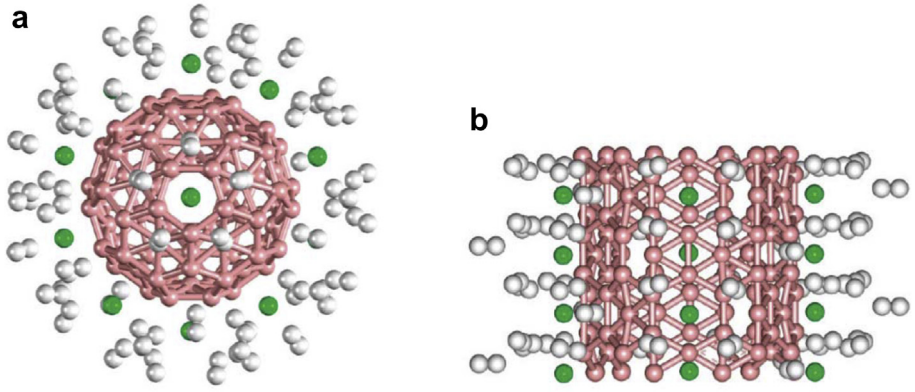

Fig. 29 – Calcium-decorated boron fullerenes storing five H_2 molecules per calcium atom showing B_{80} (left, a) and a boron nanotube (right, b) with B = pink, Ca = green and H = white. (For interpretation of the references to colour in this figure legend, the reader is referred to the web version of this article.) Reprinted from Ref. [57] with permission.

An experimental study analyzing boron-nitrogen materials found that an *h*-BN structure stored 2.6 wt% hydrogen at high temperature and pressure; the equivalent carbon structure (graphite) stored 7.4 wt%. This puts the BN material at a disadvantage relative to the carbon equivalent. However, *h*-BN desorbs H_2 at a temperature 30 K lower than graphite, which is a large asset. Research into non-carbon nanostructures is ongoing [58].

4.3. *Clathrates*

The final hydrogen adsorption system discussed in this paper is clathrates. Clathrates are chemical compounds consisting of a lattice of one compound trapping a second compound. Water (H_2O) is the most common lattice material (producing a clathrate hydrate) with the next most common being methane (Fig. 30). Ammonia, carbon dioxide and several other compounds are also possible clathrates [36,59,60].

Several gas-filled water and methane clathrates were synthesized in the late 1990's; they are described in Table 3. As can be seen, these clathrates can hold large amounts of hydrogen, but they require very high pressures. Therefore, in the early 2000's clathrates were studied again with low temperatures (77–300 K) used to form the lattice instead of high pressures [59].

This project showed some success with $H_2(H_2O)_2$, $H_2(H_2O)$ and $(H_2)_4(CH_4)$, which store 5.3, 11.2 and 33.4 wt% hydrogen respectively. This is above the 2015 DOE target of 9 wt% for $H_2(H_2O)$ and $(H_2)_4(CH_4)$. The same trend was observed with gravimetric capacities of 1.8, 3.7 and 11.1 kW h/kg respectively. These are above the 2015 target of 3 kW h/kg for $H_2(H_2O)$ and $(H_2)_4(CH_4)$. Finally, the volumetric capacities were found to be 1.5, 3.5 and 10 kW h/L respectively. Again, these are above the 2015 target of 2.7 kW h/L for $H_2(H_2O)$ and $(H_2)_4(CH_4)$; the capacity is equal to the 2010 target for $H_2(H_2O)_2$ [59].

These values appear promising, but they only occur at very high pressures and at least 2467 atm is required for synthesis. In addition, the use of methane is undesirable because one of the main reasons for switching to hydrogen fuel is to prevent further use of fossil fuels in energy production. Therefore, only hydrogen hydrates were studied further. These studies found that hydrogen hydrates have a theoretical storage capacity of 5.6 wt% hydrogen at 59–118 atm and 263 K with low energy H_2 storage and release processes. The hydrogen release energy, which is the energy required to decompose the hydrate lattice (heat of fusion), can be obtained from waste heat. In addition, hydrates have advantages in terms of cost, safety and environmental impact: hydrogen hydrates will not explode because they are self-extinguishing; they are low cost because the main component is water and sea water can be used; they are environmentally friendly because disposal costs are negligible. Unfortunately, they still require very high pressures for synthesis and operate at temperatures below the freezing point of water [36,59].

Table 3 – Hydrogen storage capacity and required pressure of several clathrates (tabulated using data from Ref. [59]).

Cage material	Solid:gas ratio	Hydrogen storage capacity (g/L H_2)	Required pressure (atm)
H_2O	1:6	23	6900
	1:1	110	21,700
CH_4	2:1	Not measured	44,400–79,000
	1:1		
	1:2		
	1:4		

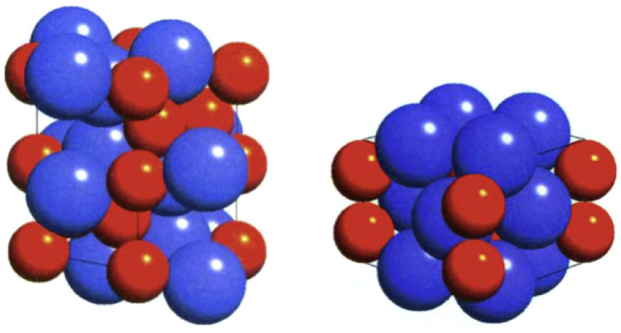

Fig. 30 – Crystal structure of $CH_4(H_2)_2$ (left) and $(CH_4)_2H_2$ (right) with the CH_4 groups represented as blue balls and the H_2 groups represented as red balls. (For interpretation of the references to colour in this figure legend, the reader is referred to the web version of this article.) Reprinted from Ref. [60] with permission.

5. Conclusion

The present paper discussed hydrogen gas storage methods from the last several decades. H_2 storage has become very important in recent years because fossil fuel resources are diminishing and the environmental harms associated with their burning are now undeniably apparent. A clean, abundant, reliable replacement is needed. Hydrogen is a good energy storage molecule, but it can only be used if H_2 containment and transportation are properly developed. The general categories of hydrogen storage discussed in this paper include mechanical techniques, such as cooling and compressing of the gas, chemical hydrides, which contain hydrogen chemically bonded to non-hydrogen atoms, and adsorption materials, which include metal-organic frameworks, carbon and other nanostructures, and clathrates. These techniques are at various stages in their development and show a wide range of gravimetric and volumetric hydrogen storage capacities. There are many encouraging theoretical results, but an experimental system capable of meeting the targets set out by the U.S. Department of Energy has not yet been found. Therefore, extensive research in this field continues.

REFERENCES

[1] Hoel M, Kverndokk S. Depletion of fossil fuels and the impacts of global warming. Resources and Energy Ecomonics 1996;18:115–36.

[2] Solomon S, Plattner G-K, Knuttic R, Friedlingstein P. Irreversible climate change due to carbon dioxide emissions. Proceedings of the National Academy of Sciences of the United States of America 2008;106(6):1704–9.
[3] Jorgensen SW. Hydrogen storage tanks for vehicles: Recent progress and current status. Current Opinion in Solid State and Materials Science 2011;15(2):39–43.
[4] Demirel Y. Energy production, conversion, storage, conservation, and coupling. In: Series: green energy and technology. Springer; 2012.
[5] Khan TI, Monde M, Setoguchi T. Hydrogen gas filling into an actual tank at high pressure and optimization of its thermal characteristics. Journal of Thermal Science 2009;18(3):235–40.
[6] Eberhardt JJ. Fuels of the future for cars and trucks. Energy efficiency and renewable energy. In: Diesel Engine Emissions Reduction (DEER) workshop San Diego, California. U.S. Department of Energy; 2002.
[7] Hua TQ, Ahluwalia RK, Peng J-K, Kromer M, Lasher S, McKenney K, et al. Technical assessment of compressed hydrogen storage tank systems for automotive applications. International Journal of Hydrogen Energy 2011;36(4):3037–49.
[8] Satyapal S, Petrovic J, Read C, Thomas G, Ordaz G. The U.S. Department of energy's national hydrogen storage project: progress towards meeting hydrogen-powered vehicle requirements. Catalysis Today 2007;120(3–4):246–56.
[9] Aceves SM, Espinosa-Loza F, Ledesma-Orozco E, Ross TO, Weisberg AH, Brunner TC, et al. High-density automotive hydrogen storage with cryogenic capable pressure vessels. International Journal of Hydrogen Energy 2010;35(3):1219–26.
[10] Zheng J, Bie H, Xu P, Chen H, Liu P, Li X, et al. Experimental and numerical studies on the bonfire test of high-pressure hydrogen storage vessels. International Journal of Hydrogen Energy 2010;35(15):8191–8.
[11] Xu P, Zheng J, Chen H, Liu P. Optimal design of high pressure hydrogen storage vessel using an adaptive genetic algorithm. International Journal of Hydrogen Energy 2010;35(7):2840–6.
[12] Doyoyo M, Faurem M. Pressure vessels with reinforcing space-filling skeletons. Journal of Pressure Vessel Technology 2008;130(3):031210.
[13] Wolf J. Liquid-hydrogen technology for vehicles. MRS Bulletin 2002;(September):684–7.
[14] Arnold G, Wolf J. Liquid hydrogen for automotive application: next generation fuel for FC and ICE vehicles. Teion Kogaku (Journal of the Cryogenic Society of Japan) 2005;40(6):221–30.
[15] Bossel U, Eliasson B, Taylor G. The future of the hydrogen economy: bright or bleak? Journal of KONES 2004;11(1-2):87–111.
[16] Crabtree GW, Dresselhaus MS, Buchanan MV. The hydrogen economy. Physics Today 2004;57(12):39–45.
[17] Ahluwalia RK, Hua TQ, Peng J-K, Lasher S, McKenney K, Sinha J, et al. Technical assessment of cryo-compressed hydrogen storage tank systems for automotive applications. International Journal of Hydrogen Energy 2010;35(9):4171–84.
[18] Paggiaro R, Bénard P, Polifke W. Cryo-adsorptive hydrogen storage on activated carbon. I: Thermodynamic analysis of adsorption vessels and comparison with liquid and compressed gas hydrogen storage. International Journal of Hydrogen Energy 2010;35:638–47.
[19] Weinberger B, Lamari FD. High pressure cryo-storage of hydrogen by adsorption at 77 K and up to 50 MPa. International Journal of Hydrogen Energy 2009;34:3058–64.
[20] Aaradahl CL, Rassat SD. Overview of systems considerations for on-board chemical hydrogen storage. International Journal of Hydrogen Energy 2009;34(16):6676–83.
[21] Gandhi K, Kumar Dixit D, Kumar Dixit B. Hydrogen desorption energies of Aluminum hydride (AlnH3n) clusters. Physica B: Condensed Matter 2010;405(15):3075–81.
[22] Jain IP, Lal C, Jian A. Hydrogen storage in Mg: A most promising material. International Journal of Hydrogen Energy 2010;35:5133–44.
[23] Jain IP, Jain P, Jian A. Novel hydrogen storage materials: a review of lightweight complex hydrides. Journal of Alloys and Compounds 2010;503(2):303–39.
[24] Ma Z, Chou MY. First-principles investigation of sodium and lithium alloyed alanates. Journal of Alloys and Compounds 2009;479:1–2.
[25] Askri F, Ben Salah M, Jemni A, Ben Nasrallah S. Heat and mass transfer studies on metal-hydrogen reactor filled with MmNi4.6Fe0.4. International Journal of Hydrogen Energy 2009;34(16):6705–11.
[26] Yoo J-H, Shim G, Park C-N, Kim W-B, Cho S-W. Influence of Mn or Mn plus Fe on the hydrogen storage properties of the Ti–Cr–V alloy. International Journal of Hydrogen Energy 2009;34(22):9116–21.
[27] Xiangqian S, Yungui C, Mingda T, Chaoling W, Gang D, Zhenzhen K. The structure and high-temperature (333 K) electrochemical performance of La0.8−xCexMg0.2Ni3.5 (x = 0.00–0.20) hydrogen storage alloys. International Journal of Hydrogen Energy 2009;34(8):3395–403.
[28] Ohoyama K, Nakamori Y, Orimo S, Yamada K. Revised crystal structure model of Li2NH by neutron powder diffraction. Journal of the Physical Society of Japan 2005;74:483–7.
[29] Wang Q, Chen Y, Gai J, Wu C, Tao M. Role of amino anion in metal amides/imides for hydrogen storage: a first principle Study. Journal of Physical Chemistry C 2008;112:18264.
[30] Umegaki T, Yan J-M, Zhang X-B, Shioyama H, Kuriyama N, Xu Q. Boron- and nitrogen-based chemical hydrogen storage materials. International Journal of Hydrogen Energy 2009;34(5):2303–11.
[31] Miwa K, Ohba N, Towata S, Nakamori Y, Orimo S. First-principles study on lithium borohydride $LiBH_4$. Physical Review B 2004;69:245120.
[32] Moysés Araújo C, Blomqvist A, Ahuja R. Ti-induced destabilization of NaBH4 from first-principles theory. Journal of Physics: Condensed Matter 2008;20(12):122202–5.
[33] Cheekatamarla PK, Finnerty CM. Reforming catalysts for hydrogen generation in fuel cell applications. Journal of Power Sources 2006;160(1):490–9.
[34] Newson E, Truong TB. Low-temperature catalytic partial oxidation of hydrocarbons (C1–C10) for hydrogen production. International Journal of Hydrogen Energy 2003;28(12):1379–86.
[35] Al-Kukhun A, Hwang HT, Varma A. A comparison of ammonia borane dehydrogenation methods for proton-exchange-membrane fuel cell vehicles: hydrogen yield and ammonia formation and its removal. Industrial & Engineering Chemistry Research 2011;50:8824–35.
[36] Di Profio P, Arca S, Rossi F, Filipponi M. Comparison of hydrogen hydrates with existing hydrogen storage technologies: Energetic and economic evaluations. International Journal of Hydrogen Energy 2009;34(22):9173–80.
[37] Chae HK, Siberio-Pérez DY, Kim J, Go YB, Eddaoudi M, Matzger AJ, et al. A route to high surface area, porosity and inclusion of large molecules in crystals. Nature 2004;427(6974):523–7.
[38] Rowsell JLC, Yaghi OM. Strategies for hydrogen storage in metal-organic frameworks. Angewandte Chemie International Edition 2005;44(30):4670–9.
[39] Rowsell JLC, Millward AR, Park KS, Yaghi OM. Hydrogen sorption in functionalized metal-organic frameworks. Journal of the American Chemical Society 2004;126:5666.
[40] Eddaoudi M, Kim J, Rosi N, Vodak D, Wachter J, O'Keeffe M, et al. Systematic design of pore size and functionality in

isoreticular MOFs and their application in methane storage. Science 2002;295(5554):469–72.
[41] Cha M-H, Nguyen MC, Lee Y-L, Im J, Ihm J. Iron-decorated, functionalized metal organic framework for high-capacity hydrogen storage: first-principles calculations. Journal of Physical Chemistry C 2010;114(33):14276–80.
[42] Wang Y, Fang M, Li Y, Liang J, Shi W, Chen J, et al. A porous 3d–4f heterometallic metal-organic framework for hydrogen storage. International Journal of Hydrogen Energy 2010;35(15):8166–70.
[43] Jordá-Beneyto M, Suárez-García F, Lozano-Castelló D, Cazorla-Amorós D, Linares-Solano A. Hydrogen storage on chemically activated carbons and carbon nanomaterials at high pressures. Carbon 2007;45(2):293–303.
[44] Ahluwalia RK, Peng JK. Automotive hydrogen storage system using cryo-adsorption on activated carbon. International Journal of Hydrogen Energy 2009;34(13):5476–87.
[45] Chen YL, Liu B, Wu J, Huang Y, Jiang H, Hwang KC. Mechanics of hydrogen storage in carbon nanotubes. Journal of the Mechanics and Physics of Solids 2008;56(11):3224–41.
[46] Assfour B, Leoni S, Seifert G, Baburin IA. Packings of carbon nanotubes – new materials for hydrogen storage. Advanced Materials 2011;23(10):1237–41.
[47] Pupysheva OV, Farajian AA, Yakobson BI. Fullerene nanocage capacity for hydrogen storage. Nano Letters 2007;8(3):767–74.
[48] Yoon M, Yang S, Wang E, Zhang Z. Charged fullerenes as high-capacity hydrogen storage media. Nano Letters 2007;7(9):2578–83.
[49] Wang L, Yang RT. Hydrogen storage properties of carbons doped with ruthenium, platinum, and nickel nanoparticles. Journal of Physical Chemistry C 2008;112(32):12486–94.
[50] Durbin, D. J., Allan N. L. and Malardier-Jugroot C. molecular hydrogen storage in fullerenes – a density functional theory study. submitted for publication
[51] Bhowmick R, Rajasekaran S, Friebel D, Beasley C, Jiao L, Ogasawara H, et al. Hydrogen spillover in pt-single-walled carbon nanotube composites: formation of stable C–H bonds. Journal of the American Chemical Society 2011;133(14):5580–6.
[52] Li Y, Yang RT. Hydrogen storage on platinum nanoparticles doped on superactivated carbon. Journal of Physical Chemistry C 2007;111(29):11086–94.
[53] Yildirim T, Ciraci S. Titanium-decorated carbon nanotubes as a potential high-capacity hydrogen storage medium. Physical Review Letters 2005;94:175501–4.
[54] Suttisawat Y, Rangsunvigit P, Kitiyanan B, Williams M, Ndungu P, Lototskyy MV, et al. Investigation of hydrogen storage capacity of multi-walled carbon nanotubes deposited with Pd or V. International Journal of Hydrogen Energy 2009;34(16):6669–75.
[55] Chandrakumar KRS, Ghosh SK. Alkali-metal-induced enhancement of hydrogen adsorption in C60 fullerene: An ab Initio Study. Nano Letters 2007;8(1):13–9.
[56] Erickson KJ, Gibb AL, Sinitskii A, Rousseas M, Alem N, Tour JM, et al. Longitudinal splitting of boron nitride nanotubes for the facile synthesis of high quality boron nitride nanoribbons. Nano Letters 2011;11:3221–6.
[57] Li M, Li Y, Zhou Z, Shen P, Chen Z. Ca-coated boron fullerenes and nanotubes as superior hydrogen storage materials. Nano Letters 2009;9(5):1944–8.
[58] Fakioğlu E, Yürüm Y, Veziroğlu TN. A review of hydrogen storage systems based on boron and its compounds. International Journal of Hydrogen Energy 2004;29(13):1371–6.
[59] Mao WL, Mao H-K. Hydrogen storage in molecular compounds. Proceedings of the National Academy of Sciences of the United States of America 2004;101(3):708–10.
[60] Somayazulu MS, Finger LW, Hemley RJ, Mao HK. High-pressure compounds in methane–hydrogen mixtures. Science 1996;271(5254):1400–2.